NASA Technical Memorandum 109159

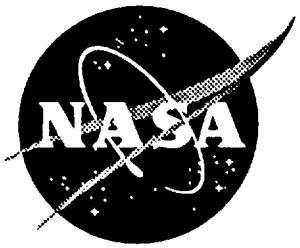

Summary of OARE Flight Calibration Measurements

Robert C. Blanchard
Langley Research Center, Hampton, Virginia

John Y. Nicholson
ViGYAN Inc., Hampton, Virginia

January 1995

National Aeronautics and
Space Administration
Langley Research Center
Hampton, Virginia 23681-0001

Summary of OARE Flight Calibration Measurements

Robert C. Blanchard
NASA Langley Research Center
Hampton, Virginia 23681-0001

John Y. Nicholson
ViGYAN, Inc.
Hampton, Virginia 23666-1325

Abstract

To date, the Orbital Acceleration Research Experiment (OARE) has flown on the Shuttle Orbiter for five missions; namely, STS-40, STS-50, STS-58, STS-62, and STS-65. The OARE instrument system contains a 3 axis accelerometer which can resolve accelerations to the nano-g (10^{-9} g) level and a full calibration station to permit *in situ* bias and scale factor calibration measurements. This calibration capability eliminates the large uncertainty encountered with accelerometers flown in the past on the Orbiter which use ground-based calibrations to provide absolute acceleration measurements. A detailed flight data report presentation is given for the OARE calibration measurements from all missions, along with an estimate of the calibration errors. The main aim is to collect, process, and present the calibration data in one archival report. These calibration data are the necessary key ingredient to produce the absolute acceleration levels from the OARE acceleration flight data.

Nomenclature

a	acceleration
A,B,C	OARE ranges, see Table 1
g	gravitational acceleration (9.80665 m/s^2)
SF	scale factor ratio, see equation (2)
X, Y, Z	sensor axes
X_b, Y_b, Z_b	Orbiter body axes
nano-g	1×10^{-9} g

Δ	reference acceleration deviation, see equation (4)
ε	error in scale factor ratio, see equation (5)
σ_t	data-trimmed standard deviation, see equation (3)
μg	1×10^{-6} g

Acronyms

MET	mission elapsed time
STS	Shuttle Transportation System

Introduction

The Orbital Acceleration Research Experiment[1] (OARE) is the third-generation Orbiter Experiment (OEX) Program accelerometer package. Its capabilities exceed both the OEX-Aerodynamic Coefficient Identification Package[2] (ACIP) and the OEX-High Resolution Accelerometer Package[3] (HiRAP) in sensitivity.

The OARE 's objective is to measure Orbiter aerodynamic performance (e.g., drag) on orbit and during the early stages of reentry and thus is purposely designed for low-frequency signals only. In addition to extracting Orbiter rarefied-flow aerodynamic performance, the OARE is used to characterize the low-frequency environment for many experiments on the Orbiter, such as those involving electrophoresis, diffusion, and crystal growth.[4] These experiments are being performed by a variety of national and international researchers.[5,6,7]

The initial developmental flight of the OARE equipment was in June 1991 on Shuttle mission STS-40.[8] This flight failed to provide reliable data due to a sensor contamination problem introduced during the manufacture process. After isolation of the problem and repair of the sensor, a second developmental flight, STS-50, occurred in July and August of 1992, which provided the first set of reliable acceleration and calibration data.[9] The OARE was flown a third time during August 1993 on Shuttle mission STS-58. The fourth and fifth flights were STS-62 and STS-65 which occurred in March 1994 and July 1994, respectively.

All interpretation of the OARE acceleration signals rely upon the calibration data which is acquired during each flight of the equipment. The accuracy with which absolute accelerations are achieved are dependent directly upon the in-flight calibration measurement accuracy. This paper

provides an in-depth discussion and results of the bias and scale factor calibration measurements performed during the orbital portion of all OARE flights to date. Included are estimates of the associated errors of both the bias and scale factor measurements.

Coordinate Systems

Figure 1 shows schematically the OARE coordinate system (X,Y,Z). Each direction corresponds to the input axes of the OARE sensor when the sensor is in its reference position and the center of the system is at the center of the proof-mass, located aft of the Orbiter's center-of-gravity. Positive X is toward the nose of the Orbiter, while positive Y is through the top of the fuselage of the Orbiter. Positive Z is out the right wing. Reference is often made to the standard aircraft body axis system (X_b,Y_b,Z_b) whose center is located at the Orbiter's center of gravity. In this system, positive X_b is toward the nose, positive Y_b is out the right wing, and positive Z_b is toward the bottom of the Orbiter fuselage. Figure 1 shows these two axes systems in relation to one another.

Instrument Overview

A brief summary of the instrument system components are provided for completeness. Reference 1 provides additional details, if required. Basically, the OARE contains a tri-axial accelerometer which uses a single free-floating (non-pendulous) electrostatically suspended cylindrical proof-mass. The accelerometer sensor assembly is attached to a microprocessor-controlled, dual-gimbal platform in order to perform in-flight calibrations. Acceleration measurements are processed and stored in the OARE flight computer memory and, simultaneously, the unprocessed data are recorded on the shuttle payload tape recorder. These payload tape recorder data are telemetered periodically to ground stations during flight.

Figure 2 is a schematic of OARE flight hardware, showing the various instrument components. The package is 43.2 x 33 x 104.1 cm (17 x 13 x 41 in.) and is mounted on a keel bridge at bay 11 on the cargo bay floor. The OARE sensor axes are co-aligned with the Orbiter body axes as shown on figure 1. The instrument weighs 53.2 kg (117 lbs) and requires 110 watts of power. The accelerometer sensor (labeled "sensor package" in Fig. 2) is attached to a moveable platform. The platform is rotated about two axes by two brushless DC torque motors.

Table 1 provides the sensor ranges, resolutions and scale factor calibration signals. There are three sensor ranges, A, B, and C. There are two rates per range to check sensor linearity. These rates are referred to as "hi"

and "lo" in the text. In addition, the calibration platform moves in two angular directions, forward and reverse, for each axis of rotation in order to detect platform motion irregularities.

In-flight Calibration

Calibration Station Overview

OARE bias and scale factor calibration data are acquired in flight using a computer-controlled, dual-gimbal rotary platform, referred to as the calibration station. A sketch of the OARE Calibration Table Assembly is shown in figure 2. The inner gimbal motor moves the sensor package attached to the platform around the inner gimbal axis to stimulate the X-axis sensor or to locate the sensor input axis in a desired direction. This is accomplished using a 16-bit optical encoder to control the platform position. Known acceleration signals can be generated to determine scale factors simply by rotating the platform at a known constant rate. In addition, biases can be determined by locating the input axis in 180° opposing directions, similar to a dividing-head used in most accelerometer calibration laboratories. The outer gimbal motor provides a similar function for the Y- and Z-axes. Both of these input axes are simultaneously stimulated during rotation about the outer gimbal axis.

Calibration Process

The OARE sensor, like all accelerometers, is affected by manufacturing tolerances and variances in physical environment including temperature and humidity, by its own inherent electronic drift, and by degradation of electronic components over time. These all impose changes to the calibration factors. Thus, periodic bias and scale factor determinations are required to assure instrument accuracy.

Together, the biases and scale factors determined from the measurements are used to obtain an absolute reference for the measured acceleration signal. The bias measurement accounts for signal offset when no signal is present; the scale factor provides a means to scale the output signal across the measurement range of the instrument. In flight, the total bias calibration takes 8 to 10 minutes (3 axes, 3 ranges) and is scheduled prior to flight. The bias measurements are processed in-flight by the programmable micro-computer and stored in the onboard OARE memory. The scale factor measurements are not processed in-flight. Since OARE has three measurement ranges, biases and scale factors are determined for each of the A-, B-, and C-ranges for each of the three axes. More information on the bias and scale factor process for the OARE is given in reference 10.

Calibration Sequence

A typical OARE flight calibration sequence for both biases and scale factors is shown in figure 3 as a function of gimble angle measurements versus mission elapsed time (MET). This is a typical half hour calibration segment during which the measurements for the biases and the scale factors for the 3 axes and the 3 ranges are performed.

Bias Sequence

The range sequence for the bias measurements is C, B, and then A. That is, the sensor is progressively forced to the higher scales, starting with the most sensitive range (C) which is the typical range for on-orbit acceleration measurements. The calibration table motion for a typical bias sequence is as follows. Data are first collected in the $0^o,0^o$ (inner and outer gimbal angles) reference position. Then the outer gimbal is changed by 180^o and data are collected for the Y- and Z-axes. Also, data are simultaneously collected for the X-axis in this position. The outer gimbal axis is brought back to reference, the inner gimbal is moved 180^o, and data are then collected for the X-axis. Six sets of processed data are recorded in memory; i.e., data sets for normal and opposite positions for all three axes. Subsequently, the sensor is placed back at the reference gimbal position and the process is repeated for the other two ranges. Thrustor firings, mechanical subsystem activities, space-craft maneuvers, satellite launches, as well as other experiment activities in the Orbiter will affect the measurements. Each data sample consists of 500 measurements (50 seconds) and a "trimmed-mean" procedure[10] is used to reduce these effects.

Scale Factor Sequence

The scale factor flight sequence also starts with the C-range, and then moves to B-, and then A-range. In a given range, the inner gimbal is moved to a mid-position of its traveling range and data are collected for the scale factor reference calculation. The platform is moved to its extreme motion limit and then rotated at a constant fixed rate until its limit in the opposite direction is encountered. Data are collected while the sensor is in motion. Next, the sensor is moved back to its mid-position and another set of reference data are collected.

The complex table motion sequence is best illustrated by considering the data collection process for the X-axis in the C-range. The corresponding gimble angles are given in figure 3. First, the sensor is moved to a position halfway through its preprogrammed slew. For example, the C-range, low-rate slew for generating scale factor calibration data requires the X-axis to travel from inner-gimbal angle of $+150^o$ to -60^o at a rate of 0.0970 radians/second

(37.8 seconds). Thus, the sensor is moved to the mid-point position of +45° and raw acceleration data are recorded for 32.2 sec. The table then moves to the inner-gimbal starting position of +150° and slews at the prescribed rate until -60° is reached. This second set of acceleration data are recorded also for 32.2 seconds during this slew. Some time is allowed for sensor settling. Subsequent to this, the inner-gimbal angle is reset to mid-position and a third set of data are recorded. This sequence is performed again for the X-axis at a higher rate. (It is difficult to see the change in slope for the higher rate in figure 3 due to the choice of graphing scales.) The process is repeated for the Y- and Z-axes by holding the inner gimbal angle at zero while changing the outer gimbal angle.

Once the data have been collected for the 3 axes in the C-range for the 2 rates, the whole process is repeated for the B- and A-range as indicated in figure 3. Unlike the bias data, the data collected for scale factor calculations are not processed in flight. The example shown in figure 3 is for a reverse direction platform motion. Throughout the mission, the platform is alternately rotated in the opposite direction producing both forward and reverse direction scale factors. Alternate table directions provide a means to check the table for irregularities.

Calibration Results

Bias Calibration Results

Bias calibrations are shown in figures 4 through 15 for all instrument ranges (A, B, and C), for all missions (STS-50, 58, 62, and 65), and for OARE instrument axes (X, Y, and Z). STS-40 data, which gave unsatisfactory results due to a sensor problem[8], are not included in this report. Each figure shows the results for all three axes for a given range and mission. All missions for a given range are grouped together. A figure index guide is placed on a separate page before the bias measurement results to facilitate finding a given data set. Each graph encompasses the OARE biases during the entire mission and the abscissa is given in multiple units of days. The ordinate scales are adjusted to best illustrate the bias data and care should be taken when comparing different figures.

Each bias measurement on each figure contains an error bar. This error bar is calculated as follows. Each processed data point (used in determining a given bias) has an associated error which is given by

$$\frac{\sum_{n} |a_i - \bar{a}|}{n} \qquad (1)$$

where a_i are the acceleration values, $\bar{a}$ is the "trimmed" acceleration mean, and n is the number of points after trimming the preset 500 data point sample size. This is the average absolute deviation of the trimmed data set from the trimmed mean. This is the preprogrammed measure of error used by the OARE microprocessor during each flight. This measure of error is converted to a standard deviation, σ, by assuming a Gaussian distribution and the error bars shown on each figure are next calculated by an application of the Central Limit Theorem.[11] (NOTE: these error bars tend to underestimate the actual errors due to the "trimming" process.) In addition, each axis of each figure includes the average error (labeled "Av. Error") which is the mean of the errors over the entire flight.

Bias Measurement Comparisons

The bias measurement data discussed previously are arranged by instrument range (A, B, and C) then by mission (STS-50, 58, 62, and 65). Each figure contains synchronized graphs of the three instrument axes (X, Y, and Z) for the entire mission. An index page precedes this group of data as an additional guide. Comparisons of bias data between instrument ranges, axes, and flights provide insights into the sensor characteristics, the calibration stability, and, most importantly, the degree of precision. Figures 4 through 15 represent all the flight bias measurements and provide a data base for future application of calibration data. Some observations are included in this section of the report. However, these comments are not necessarily inclusive, since the primary thrust of this report is to collect, process, and present the calibration data in one archival report.

There is a significant change in the X-axis bias levels on STS-65 from the previous flights. This is primarily due to electronic component changes prior to this flight (due to a post-flight electronic failure on STS-62) and partially due to colder operating temperatures during this flight when compared to previous flights.

There is typically a larger variation in the bias signal in all axes several days prior to the end of the mission without much change in the measurement errors. Figure 6 is a good example of this phenomenon. The explanation is that the Orbiter is more active in orientation maneuvers compared to the rest of the mission which is devoted to payload scientific investigations at a constant attitude. These orientation maneuvers and preparations for reentry affect the calibration assumptions by providing a

changing environment. This is not factored into the measurement statistics, but clearly impacts accuracy and any absolute acceleration calculations using these bias measurements.

As expected, the variation in biases increases from range C to B to A since 1 count represents increasingly larger acceleration increments. Certain behavior not anticipated before flight also occur, such as the large drift for the Z-axis, A-range from 0 to 96 hours; see figure 4.

It is clear that the standard error is a function of the OARE internal electronic filters. The X-axis errors are three times larger than the Y/Z-axes. But this is due to the internal electronic smoothing process intentionally introduced in the Y/Z-axes subsequent to STS-50 to eliminate the platform "jitter" along these axes during scale factor activities. Table 2 gives the bias error (in μg's) averaged over missions for each range and axis. This provides a rough gauge of the precision of the bias calibrations for each case.

The biases for all ranges and axes for STS-65 (see Figs. 7, 11, and 15) exhibits a "cupped" effect with the X-axis showing the more predominant effect. This is probably due to the temperature profile encountered by the instrument during this flight. This will be discussed next.

Bias Temperature Sensitivity Results

Figures 16, 17, and 18 show the bias measurements as a function of measured temperature (^{o}C) for all instrument ranges, axes, and missions. The bias measurements at the beginning of the mission have been eliminated, where appropriate, for these graphs in order to eliminate the obvious initial time dependent effects. Typically, about 48 hours are required for achieving bias measurement stability in the X-axis. Each bias data set (e.g., for a given range, axis, and mission) have been fit with a linear function in order to obtain the bias temperature sensitivity coefficient for the entire mission. This average temperature coefficient provides a measure of how much bias changes per unit change in temperature over the entire flight. In some cases (for example, on STS-65, Z-axis; see Fig. 16), a linear fit does not reflect the instrument temperature sensitivity behavior at cold temperatures. Thus, the slope of the fit is only a first order comparative measure. The values of the slope of the fit are included on each figure as a table in the upper right hand corner of each axes. Table 3 is a summary of the average temperature sensitivity coefficient for the entire data set. This provides a quick reference to the approximate temperature dependence of the OARE sensor for each axis, range, and mission.

There are several comments worth mentioning about the bias data temperature dependence. First, in general, the small values for the bias

temperature coefficients make this sensor ideal for low-frequency (e.g., drag) acceleration measurements. Except for STS-65, there is good stability of bias measurements between missions in all axes for the C-range. The reason for the STS-65 behavior is readily explained by the rework of the electronics prior to flight. The other ranges show some inconsistencies between missions (e.g., see Fig. 16, A-range, Z-axis). There are other features, such as a spread of biases for a given temperature which can be seen on all figures.

Scale Factor Calibration Results

As discussed, the on-orbit scale factor calibration of each sensor axis is accomplished by rotating the proof-mass at known rates about one of the two gimbal axes (i.e., the inner-gimbal axis for X-axis calibration and outer-gimbal axis for Y/Z-axes calibration). The distances from gimbal axes to proof-mass are known accurately (about 0.08 mm) and the rotation rates are accurately controlled; thus, the calibration acceleration signal can be calculated within a fraction of one percent. This calibration input signal is referred to as the "theoretical" signal.

In principle, the reference value obtained when the sensor is not rotating is subtracted from the measured acceleration during rotation. This difference provides the relative acceleration amplitude generated by the platform motion. This amplitude, referred to as the "measured" acceleration, is compared to the theoretical acceleration to define the scale factor ratio, SF, that is,

$$SF = a_{theor}/a_{meas} \qquad (2)$$

A scale factor ratio value of unity corresponds to the count conversion factors being exactly equal to the theoretical signal produced by the platform rotation. The SF is used as a multiplier adjustment to the acceleration measurements made during flight after removing the bias.

Figures 19 through 30 are the scale factor ratio measurement results for all instrument ranges, missions, and axes. The organization of the scale factor results is similar to the bias results previously presented. That is, for a given range, the data are given as a function of mission with the data for all three axes shown for the entire mission on one page. As before, an index guide on a separate page is provided to facilitate finding specific data sets. For scale factor measurements there are two additional discriminators; namely, angular rates and angular direction, both of which have two different values per axis per range. In addition, unlike the bias calculations which are processed during the flight, all scale factor calculations are performed post-flight using the data stored in memory during the flight.

The scale factor measurements on the Orbiter are a technical challenge and, to date, success has progressed with each successive flight. The problems encountered are numerous, including upsetting the sensor to inducing low frequency disturbances (i.e., "jitter") by the table motion itself. For example, no scale factor data on the C-range was acquired on STS-50 in the Y- and Z-axes due to the large table induced disturbances. But, as seen in figure 30, STS-65, most of the problems associated with obtaining scale factor measurements have been resolved. All scale factor problems have been associated with the most sensitive C-range. Even in the presence of these problems, however, some useful calibration data were obtained by utilizing a different data analysis approach (see Ref. 10).

Some unexplained characteristics of the scale factor measurements are as follows. The Y-axis, A-range scale factor values for forward and reverse directions are consistently different by about 7 percent for all missions. Similarly, anomalous results were obtained for the Z-axis on STS-50 and STS-58. There is no clear explanation other than mechanical motion differences. This and other hypotheses need further exploration.

For the B-range, the Y-axis performed much the same as the A-range with the differences being about 5 percent. Anomalous results for the Z-axis for STS-50 and STS-58 were also encountered on the B-range. Also, some C-range scale factors are unrealistic, for example, see figure 28, Z-axis.

Table 4 gives a summary of the scale factor ratio measurements averaged over an entire mission. That is, there is a representative number for each mission, range, axis, table direction, and rate. As is seen, these averages are consistent from flight to flight with only slight departures for STS-65. As expected, the averages for the Z-axis, C-range on STS-58 are unrealistic. The reverse direction scale factor ratios for this case have been calculated by a unique method specifically designed for that axis on that flight (see Ref. 10) and yield average values of 1.11 and 1.17 for the low and high rates, respectively.

Scale Factor Measurement Errors

The errors associated with the preceding scale factor ratio measurements are given in figures 31 through 42. These errors are presented separately from the scale factor ratio data because the scale factor graphs become too cluttered when error bars are inserted. As previously, a separate index page prior to the figures is given to quickly identify a given data set.

The errors for the scale factor calculations are obtained as follows. The total standard deviation of the "trimmed" data sets is given by,

$$\sigma_t = \sqrt{\frac{\sigma_1^2}{n_1} + \frac{\sigma_2^2}{n_2} + \frac{\sigma_3^2}{n_3} + \Delta^2} \qquad (3)$$

where σ_1, σ_2, and σ_3 are the standard deviations for the trimmed data set in the intervals pre-, during, and post-rotation rates, respectively. The n_1, n_2, and n_3 are the number of data points after trimming in the aforementioned intervals. The Δ term depends upon the pre- and post-rate average accelerations, a_1 and a_3, as follows,

$$\Delta = \frac{a_1 - a_3}{2} \qquad (4)$$

Thus, the error, ε is given by,

$$\varepsilon = \frac{\sigma_t \cdot SF}{\left| a_2 - \frac{a_1 + a_3}{2} \right|} \qquad (5)$$

The standard deviation, σ_t of equation (3) takes into account the errors of the three measurement regions used in determining the scale factor ratio. The effect of any differences in the average accelerations due to spacecraft activity in the regions for the pre- and post-rotation rate are also included by the addition of the Δ term. Finally, equation (5) scales the standard deviation so that it represents the error in the measured scale factor ratios shown in figures 19 through 30.

A brief summary of the errors associated with scale factor ratio measurements are as follows. The A- and B-range error determinations are roughly at the 0.5 percent level for all axes. There are several exceptions as can be seen in the figures (e.g., Fig. 33, STS-62, X-axis, hi-rate, forward direction). Similarly, the C-range X-axis scale factor determinations are on the order of 1.5 to 2.0 percent. The Y- and Z-axes in the C-range have continued to be a problem throughout all the missions and the errors quantify the degree of difficulty. Neither the Y- or Z-axis scale factor in the C-range could be achieved during STS-50 due to "jitter" of the calibration table as it moved. Reworking the system electronics gave acceptable C-range Y-axis scale factors for STS-58, but not for the Z-axis. As can be seen in figure 28, "trimmed" data gave unrealistic results mostly between 2.0 and 4.0. Satisfactory scale factor results of the Z-axis for STS-58 have been achieved by more complicated means (see Ref. 10), but only for the reverse direction. This limitation is supported by the scale factor errors for this axis seen in figure 40. However,

the errors and the scale factor results for both Y- and Z-axis for the C-range improve in STS-62 and STS-65.

Table 5 is constructed similar to Table 4, except that it contains the mission average scale factor ratio errors. As before, the errors are averaged over an entire mission and are listed in the table for each mission, range, axis, table direction, and rate. The average errors change somewhat from flight to flight, but do not reach 1 percent in the A- or B-range. The error values in the C-range are generally around one and are all less than 3 percent for the X- and Y-axis. The Z-axis errors for STS-58 are considerably higher. Marked improvement is seen for STS-62 and STS-65.

Summary

The Orbital Acceleration Research Experiment (OARE), a tri-axial, electrostatically suspended, single proof-mass accelerometer system with nano-g sensitivity and in-flight calibration capability has flown on STS-40, STS-50, STS-58, STS-62, and STS-65, spanning a time period of about 2 years. The OARE has complete calibration capabilities in order to provide data for both bias and scale factor determinations. Bias data are processed in-flight and stored in the OARE computer memory, while data generated for scale factor calculations are stored for post-flight processing.

The primary purpose of this report is to collect, process, and present the calibration data in one archival report. All bias and scale factor measurements for STS-50, 58, 62, and 65 are presented graphically. Estimates of errors for each calibration are also given. An index page is utilized in the presentation to facilitate finding a specific set of calibration data. In addition, the bias temperature dependencies for these missions are presented.

Bias and scale factor measurements provide the means to produce absolute acceleration measurements. However, as with any measurements, both bias and scale factor determinations have uncertainties associated with them. Thus, the determination of the absolute acceleration is known to within certain limits which are a direct function as to how well both the bias and scale factors have been determined.

References

[1]Blanchard, R. C., Hendrix, M. K., Fox, J. C., Thomas, D. J., and Nicholson, J. Y.: "The Orbital Acceleration Research Experiment," Journal of Spacecraft and Rockets, vol. 24, no. 6, Nov.-Dec. 1987, pp. 504-511.

[2]Anon, ACIP/HiRAP End Item Specification, Drawing No. 3291583, Bendix Corp., Aerospace Systems Div., Ann Arbor, MI, May 1982.

[3]Blanchard, R. C.; and Rutherford, J. F.: "The Shuttle Orbiter High Resolution Accelerometer Package Experiment: Preliminary Flight Results." Journal of Spacecraft and Rockets, vol. 22, no. 4 July-August 1985, p 474.

[4]NASA Office of Space Science and Applications: "Microgravity Science and Applications Program Tasks," 1991 revision, NASA TM-4349, February 1992.

[5]Ott, R.: "NASA's Commercial Microgravity Program," AIAA 93-0371, January 1993, Nevada.

[6]Wetter, Barry: "Canada's Microgravity Science Program," AIAA 93-0372, January 1993, Nevada.

[7]Latorre, R. and Mims, J.: "Soviet Approach to Space Manufacturing in Microgravity," AIAA 93-0375, January 1993, Nevada.

[8]Blanchard, R. C., Nicholson, J. Y., and Ritter, J. R.: "STS-40 Orbital Acceleration Research Experiment Flight Results During a Typical Sleep Period," Microgravity Science and Technology, vol. 2, 1992, pp. 86-93.

[9]Blanchard, R. C., Nicholson, J. Y., and Ritter, J. R.: "Preliminary OARE Absolute Acceleration Measurements on STS-50," NASA TM-107724, February 1993.

[10]Blanchard, R. C., Nicholson, J. Y., Ritter, J. R. and Larman, K. T.: "OARE Flight Maneuvers and Calibration Measurements on STS-58," NASA TM-109093, Apr. 1994.

[11]Snadecor, George W. and Cochran, William G.: "Statistical Method," 7th ed., Iowa State University Press, 1980, pp. 45-50.

Table 1 OARE Sensor Range, Resolution, and Scale Factor Calibration Signals

RANGE & RESOLUTION		
Range	X-AXIS	Y,Z-Axis
	Full Scale (10^{-6} g)	
A	10000	25000
B	1000	1970
C	100	150
	Resolution (10^{-9} g)	
A	305.00	763.0
B	30.50	58.0
C	3.05	4.6

SCALE FACTOR CALIBRATION			
	Range	Cal. Signals (μg)	Date Collection Time (sec)
X Axis			
	A	850.7	7.0
	A	425.3	11.0
	B	850.7	6.7
	B	425.3	10.7
	C	45.02	21.5
	C	20.01	32.2
Y,Z Axis			
	A	1392.1	7.0
	A	695.9	11.0
	B	1207.6	7.4
	B	530.6	12.6
	C	67.2	22.5
	C	49.5	26.5

Table 2. MISSION AVERAGE BIAS ERROR (μg) SUMMARY

STS	AXIS	X			Y			Z		
	RANGE	A	B	C	A	B	C	A	B	C
Jun 92' 50		0.204	0.221	0.297	0.142	0.214	0.086	0.179	0.141	0.081
Oct 93' 58		0.213	0.237	0.214	0.206	0.194	0.075	0.222	0.186	0.089
Mar 94' 62		0.199	0.169	0.160	0.289	0.117	0.044	0.190	0.087	0.044
Jul 94' 65		0.225	0.257	0.237	0.236	0.197	0.087	0.209	0.156	0.081
	FLT AV.	0.218	0.221	0.227	0.218	0.181	0.073	0.200	0.143	0.074

Table 3. AVERAGE TEMPERATURE SENSITIVITY COEFFICIENT (μg/oC) SUMMARY

DATE STS	AXIS	X			Y			Z		
	RANGE	A	B	C	A	B	C	A	B	C
Jun 92' 50		-0.053	-0.048	-0.032	0.540	0.056	0.027	-0.275	-0.021	-0.016
Oct 93' 58		-0.014	-0;002	-0.019	0.605	0.056	0.027	-0.186	-0.021	-0.016
Mar 94' 62		-0.152	-0.016	+0.007	0.724	0.047	0.010	-0.234	-0.029	-0.013
Jul 94' 65		-0.089	-0.070	-0.065	0.614	0.052	0.015	-0.049	0.015	0.016
	FLT AV	0.077	-0.034	-0.027	0.621	0.053	0.020	-0.186	-0.014	-0.007

Table 4. MISSION AVERAGE SCALE FACTOR RATIO MEASUREMENTS SUMMARY

A-Range

		X				Y				Z			
		hi		lo		hi		lo		hi		lo	
Fig.	Flt.	for.	rev.	for.	rev.	for.	rev.	for.	rev.	for.	rev.	for.	rev.
19	50	1.03	1.04	1.03	1.04	1.17	1.09	1.16	1.10	1.08	1.12	1.09	1.12
20	58	1.04	1.04	1.03	1.04	1.16	1.09	1.15	1.10	1.10	1.11	1.11	1.13
21	62	1.03	1.03	1.03	1.03	1.15	1.09	1.15	1.10	1.09	1.09	1.09	1.10
22	65	1.06	1.07	1.07	1.07	1.18	1.13	1.17	1.13	1.11	1.11	1.11	1.12

B-Range

		X				Y				Z			
		hi		lo		hi		lo		hi		lo	
Fig.	Flt.	for.	rev.	for.	rev.	for.	rev.	for.	rev.	for.	rev.	for.	rev.
23	50	1.02	1.03	1.02	1.03	1.16	1.11	1.14	1.11	1.11	NA	1.13	1.17
24	58	1.02	1.02	1.02	1.02	1.15	1.11	1.14	1.10	1.12	1.13	1.15	1.17
25	62	1.02	1.02	1.02	1.02	1.15	1.10	1.14	1.11	1.10	1.10	1.12	1.12
26	65	1.06	1.06	1.06	1.05	1.18	1.15	1.17	1.15	1.12	1.13	1.13	1.14

C-Range

		X				Y				Z			
		hi		lo		hi		lo		hi		lo	
Fig.	Flt.	for.	rev.	for.	rev.	for.	rev.	for.	rev.	for.	rev.	for.	rev.
27	50	1.03	1.04	1.03	1.03	NA	NA	NA	NA	NA	NA	NA	NA
28	58	1.02	1.02	1.01	1.00	1.17	1.13	1.17	1.13	2.90	2.07	2.92	2.68
29	62	1.02	1.02	1.01	1.00	1.15	1.13	1.16	1.13	1.39	1.27	1.38	1.31
30	65	1.06	1.04	1.05	0.97	1.16	1.16	1.16	1.15	1.35	1.36	1.42	1.43

Table 5. Mission Average Scale Factor Measurements Errors Summary

A-Range

		X				Y				Z			
		hi		lo		hi		lo		hi		lo	
Fig.	Flt.	for.	rev.	for.	rev.	for.	rev.	for.	rev.	for.	rev.	for.	rev.
31	50	.0013	.0012	.0017	.0020	.0050	.0046	.0062	.0042	.0036	.0022	.0053	.0027
32	58	.0010	.0010	.0018	.0016	.0042	.0040	.0055	.0035	.0038	.0031	.0074	.0049
33	62	.0046	.0008	.0020	.0011	.0041	.0031	.0029	.0030	.0020	.0015	.0041	.0020
34	65	.0023	.0024	.0030	.0038	.0043	.0047	.0042	.0033	.0033	.0027	.0042	.0027

B-Range

		X				Y				Z			
		hi		lo		hi		lo		hi		lo	
Fig.	Flt.	for.	rev.	for.	rev.	for.	rev.	for.	rev.	for.	rev.	for.	rev.
35	50	.0012	.0013	.0021	.0018	.0041	.0030	.0042	.0039	.0021	.0010	.0095	.0017
36	58	.0008	.0011	.0014	.0013	.0035	.0022	.0031	.0025	.0024	.0015	.0061	.0029
37	62	.0026	.0007	.0017	.0012	.0029	.0039	.0024	.0020	.0021	.0010	.0033	.0013
38	65	.0018	.0019	.0036	.0028	.0048	.0033	.0035	.0035	.0023	.0012	.0034	.0021

C-Range

		X				Y				Z			
		hi		lo		hi		lo		hi		lo	
Fig.	Flt.	for.	rev.	for.	rev.	for.	rev.	for.	rev.	for.	rev.	for.	rev.
39	50	.0103	.0115	.0194	.0199	NA	NA	NA	NA	NA	NA	NA	NA
40	58	.0081	.0083	.0147	.0120	.0064	.0060	.0094	.0056	.1760	.0481	1.40	.0673
41	62	.0063	.0075	.0254	.0107	.0062	.0051	.0093	.0044	.0123	.0083	.0972	.0076
42	65	.0169	.0122	.0292	.0211	.0132	.0088	.0265	.0074	.0317	.0077	.0815	.0112

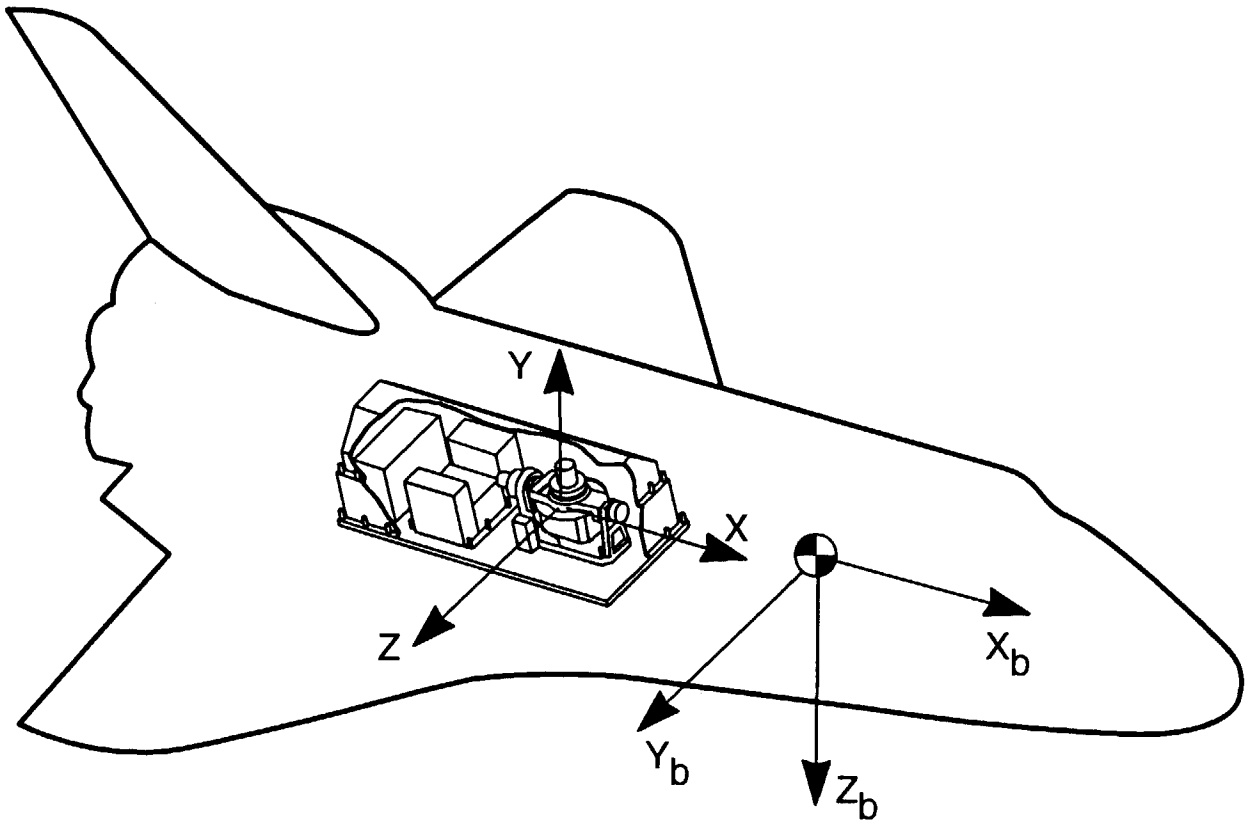

Fig. 1 OARE (X, Y, Z) and Orbiter body axes (X_b, Y_b, Z_b) coordinate systems.

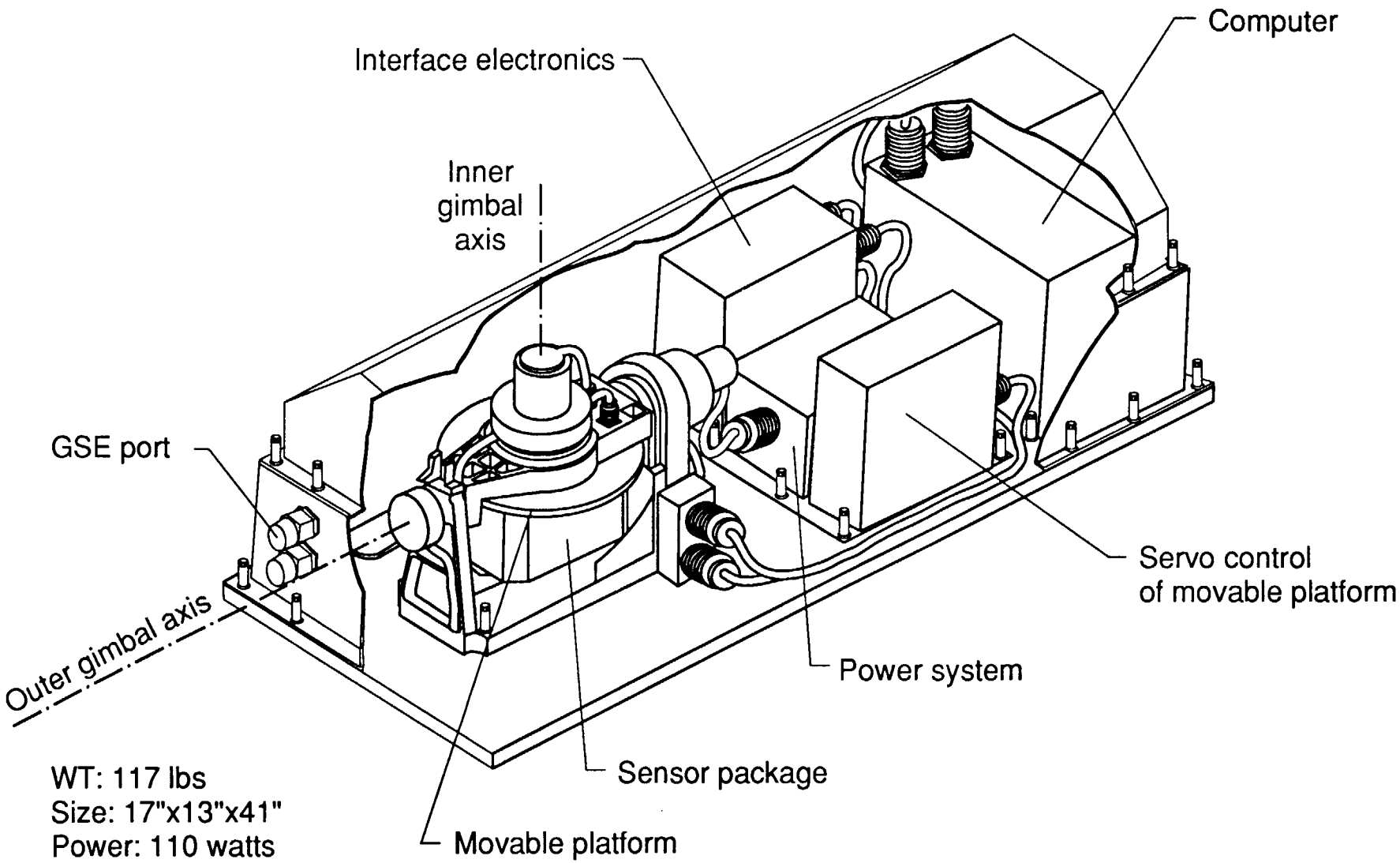

Fig. 2 OARE packing layout sketch.

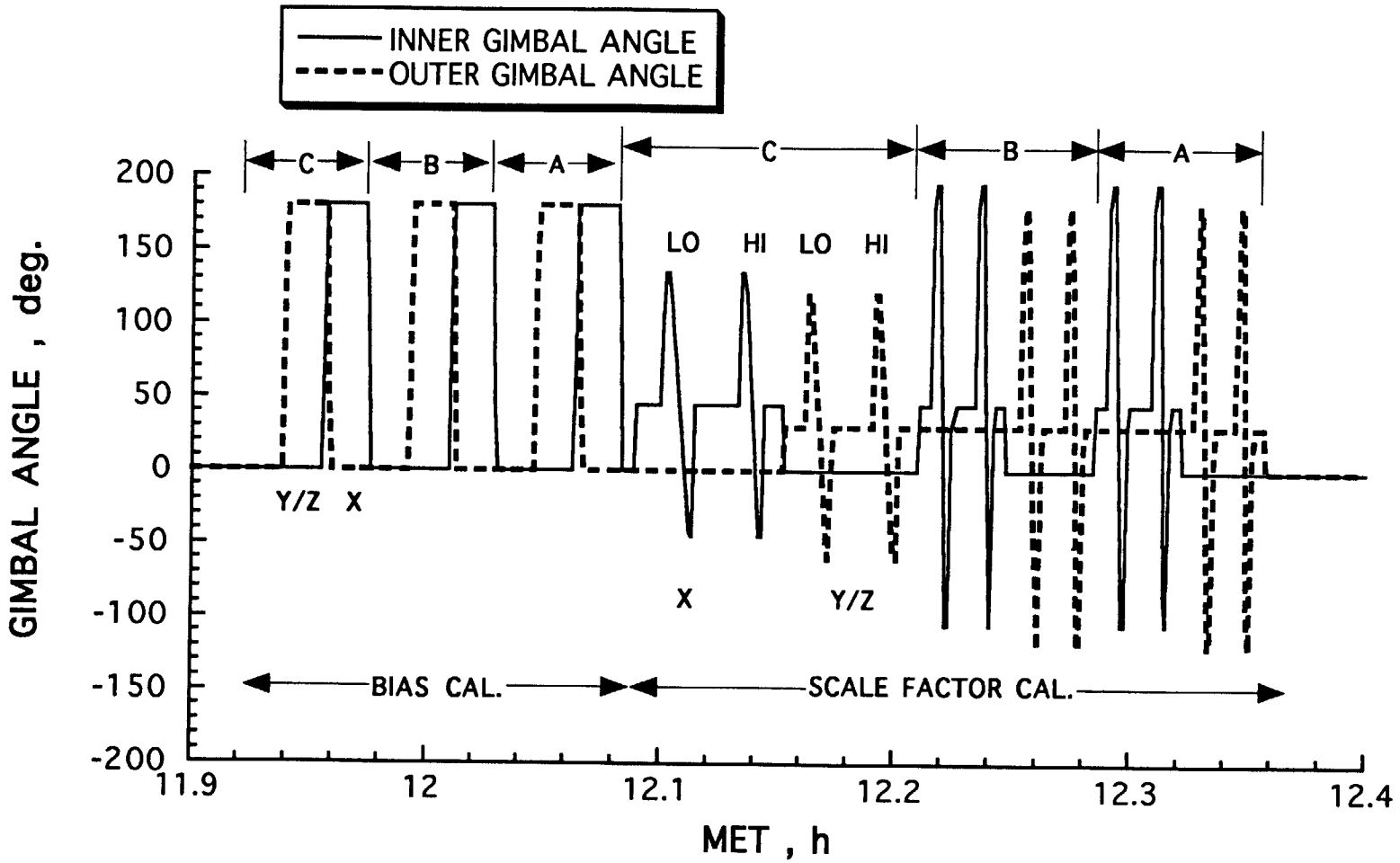

Fig. 3 Typical inner and outer gimbal angle measurements during a calibration sequence.

BIAS MEASUREMENT INDEX

FIG.	RANGE	MISSION	AXES
4	A	STS-50	X,Y,Z
5		-58	"
6		-62	"
7		-65	"
8	B	STS-50	X,Y,Z
9		-58	"
10		-62	"
11		-65	"
12	C	STS-50	X,Y,Z
13		-58	"
14		-62	"
15		-65	"

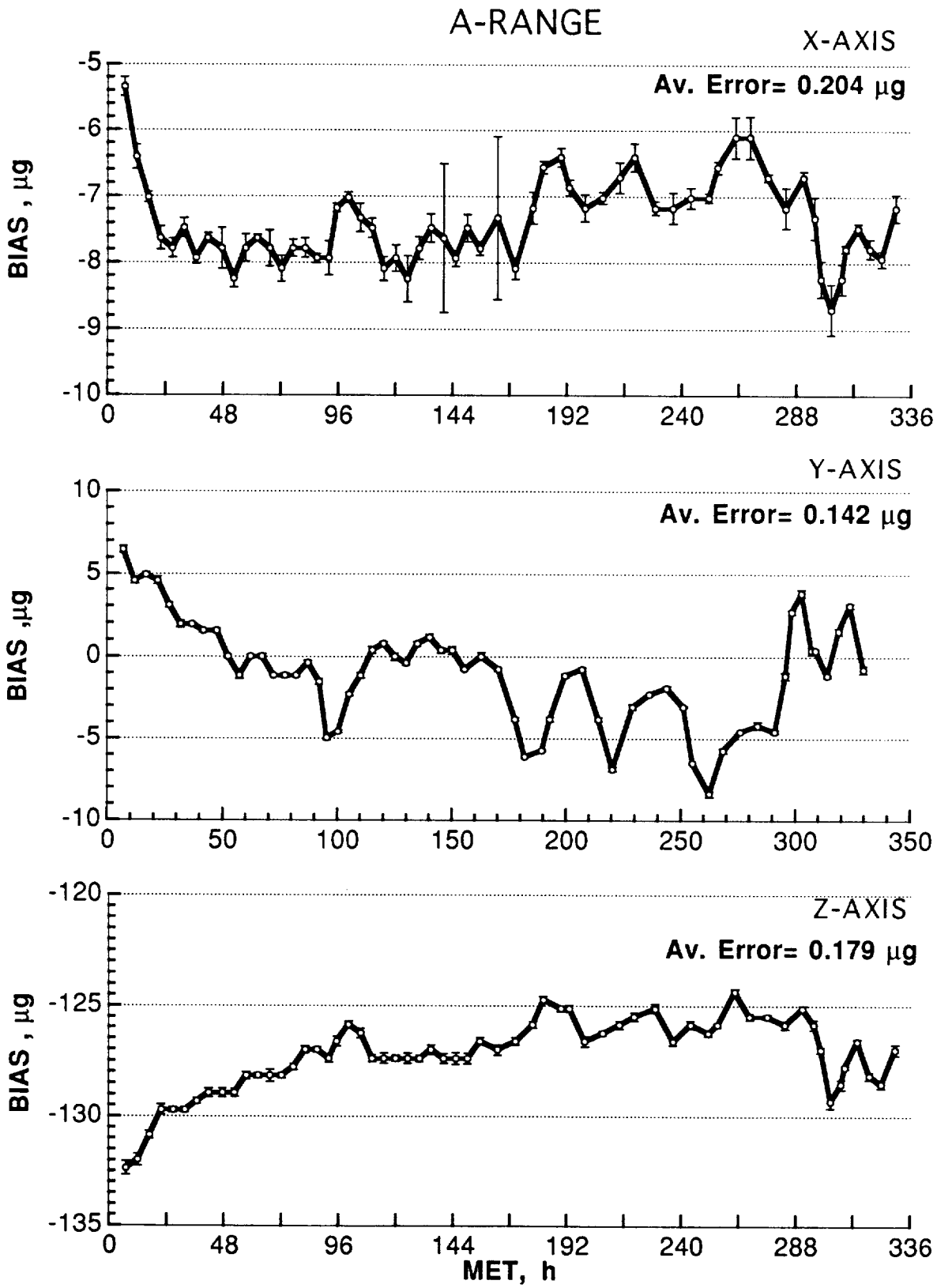

Fig. 4 OARE STS-50 A-range bias measurements with error bars.

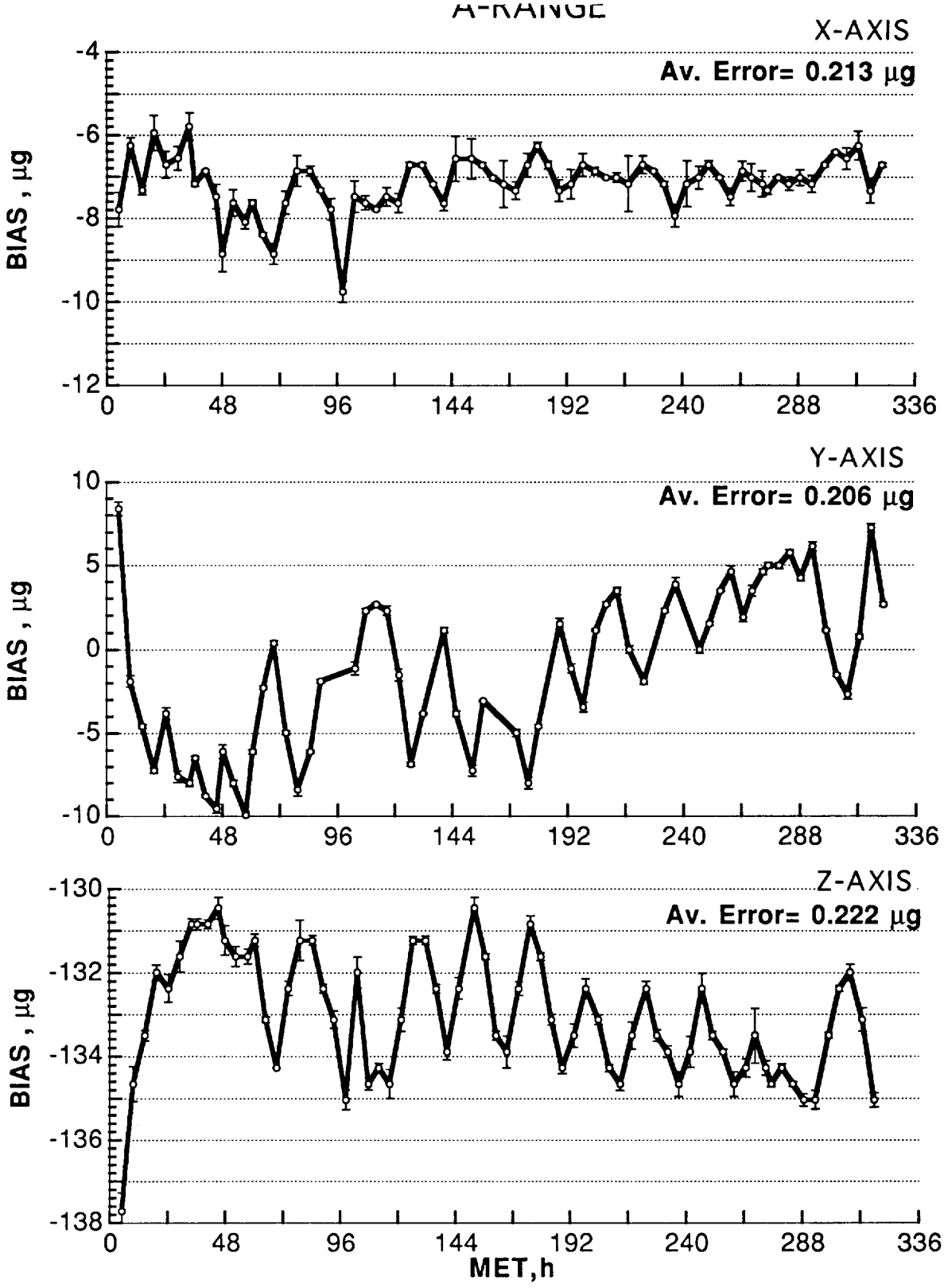

Fig. 5 OARE STS-58 A-range bias measurements with error bars.

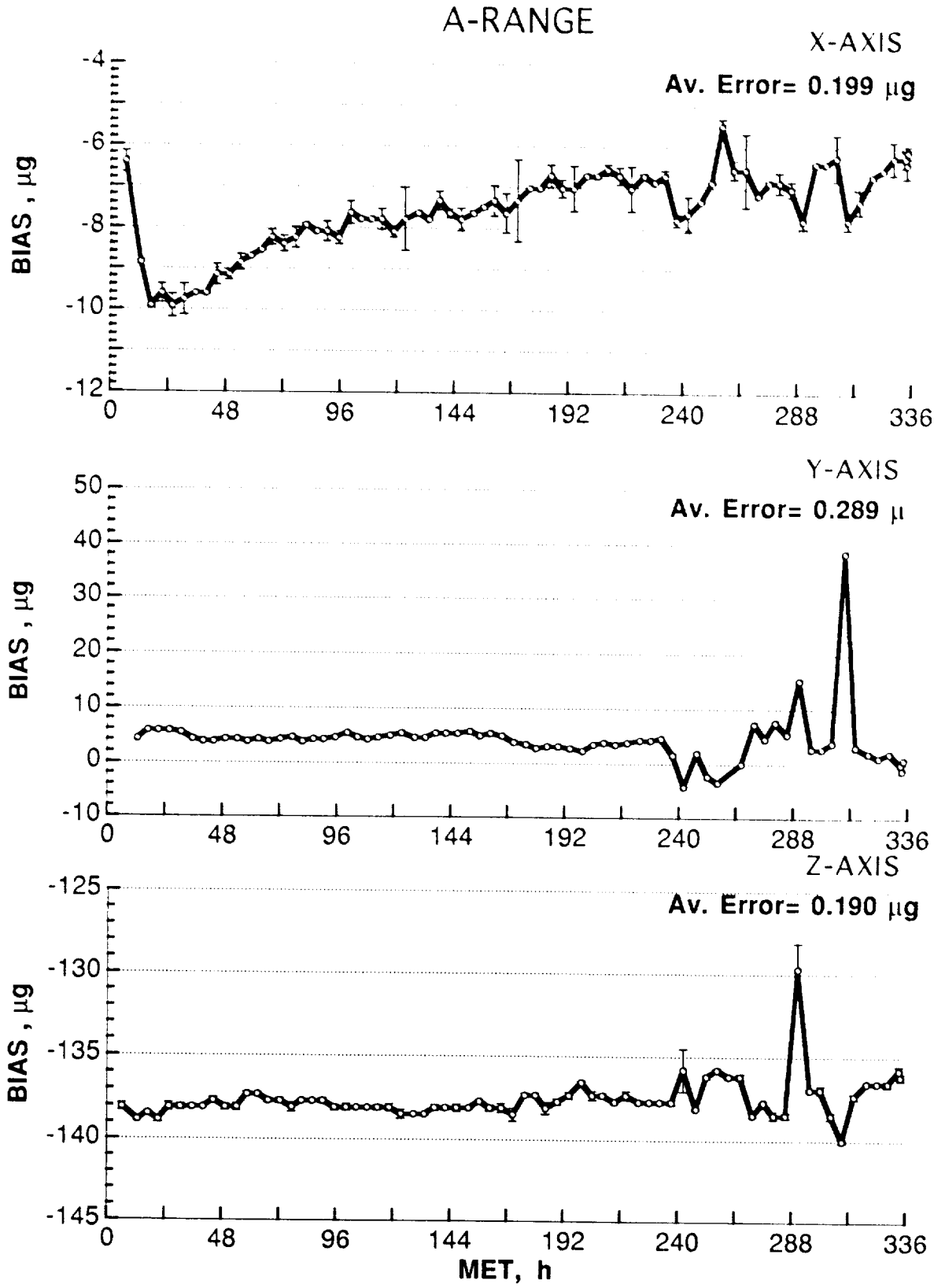

Fig. 6 OARE STS-62 A-range bias measurements with error bars.

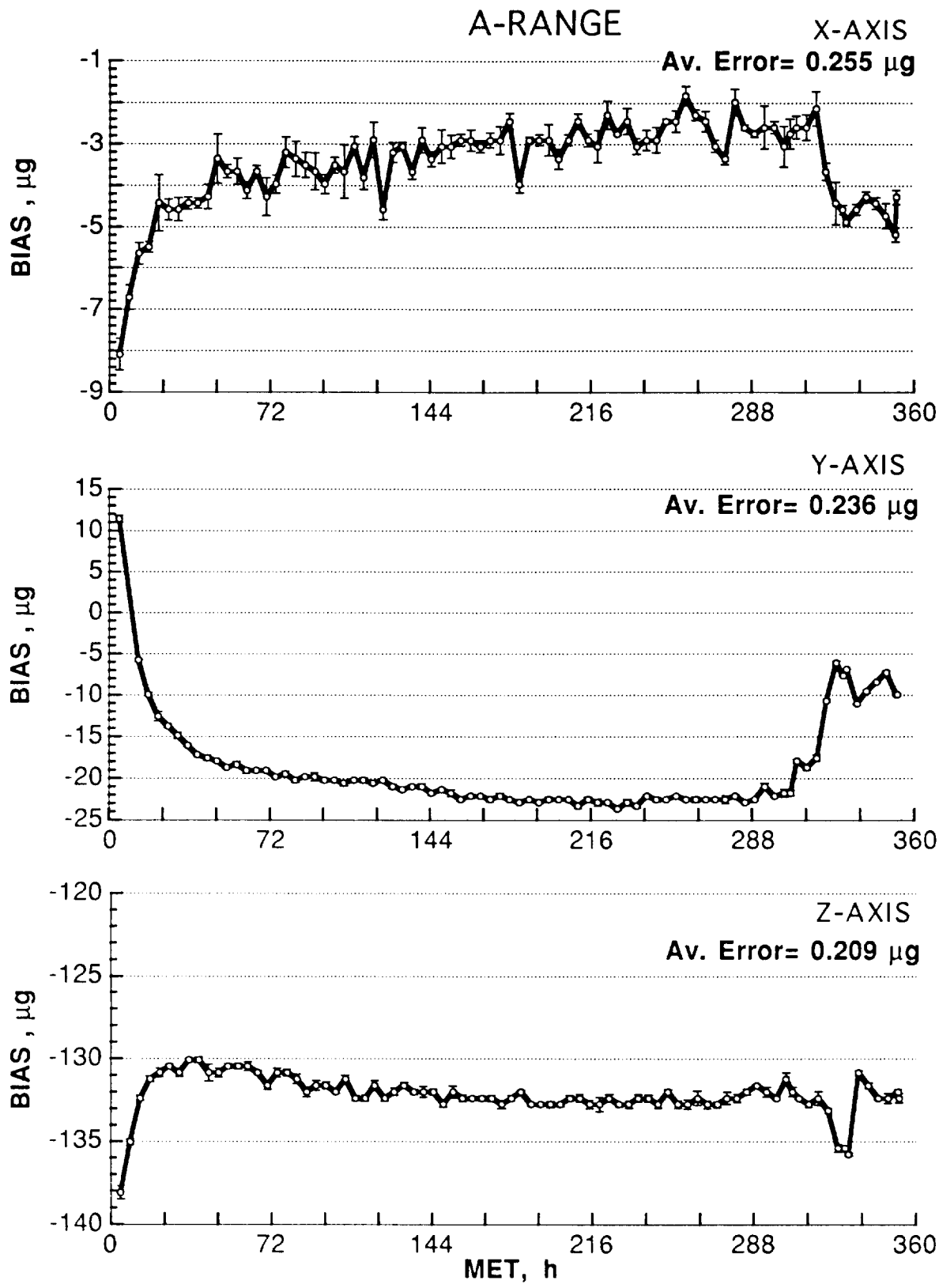

Fig. 7 OARE STS-65 A-range bias measurements with error bars.

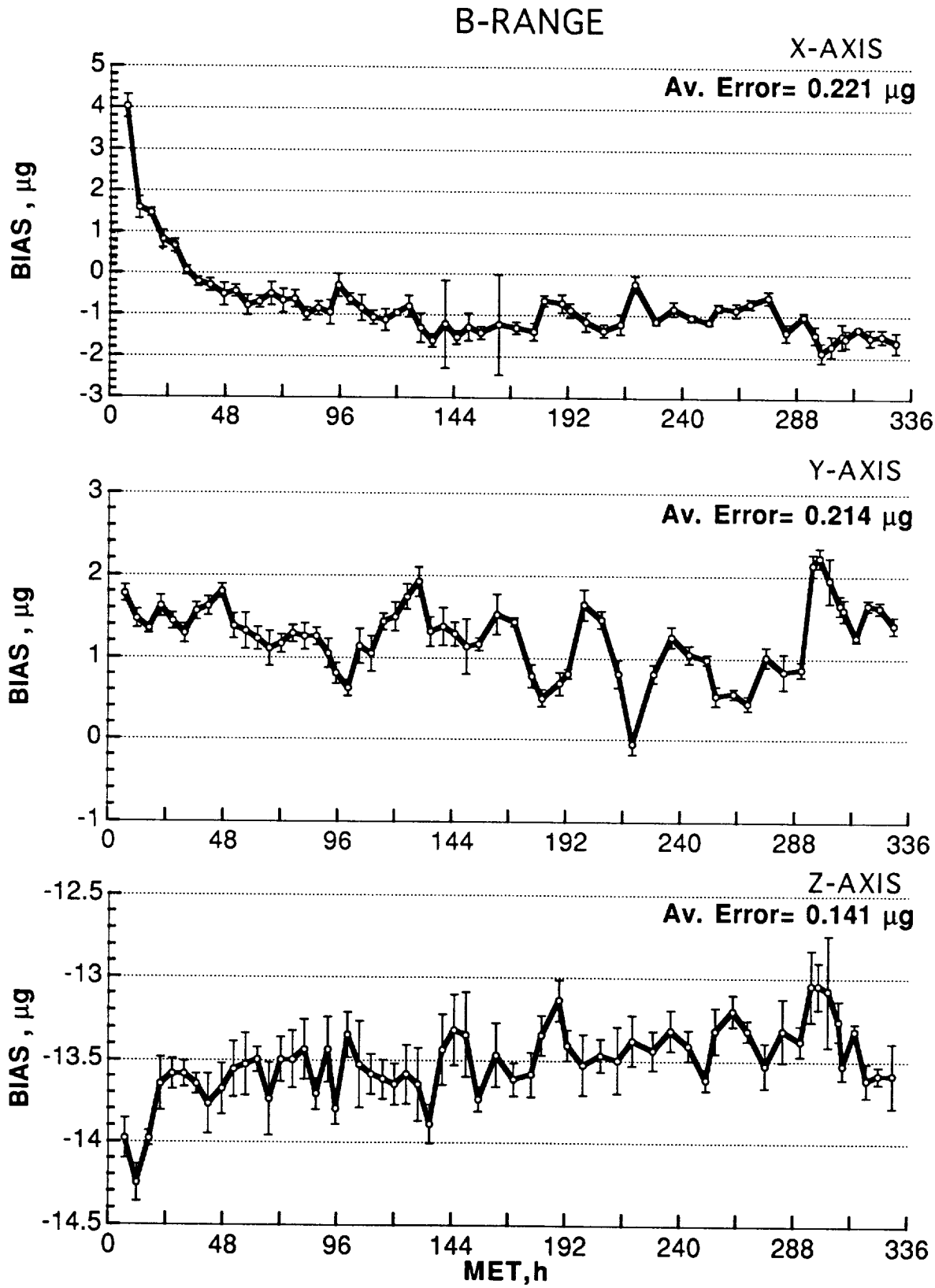

Fig. 8 OARE STS-50 B-range bias measurements with error bars.

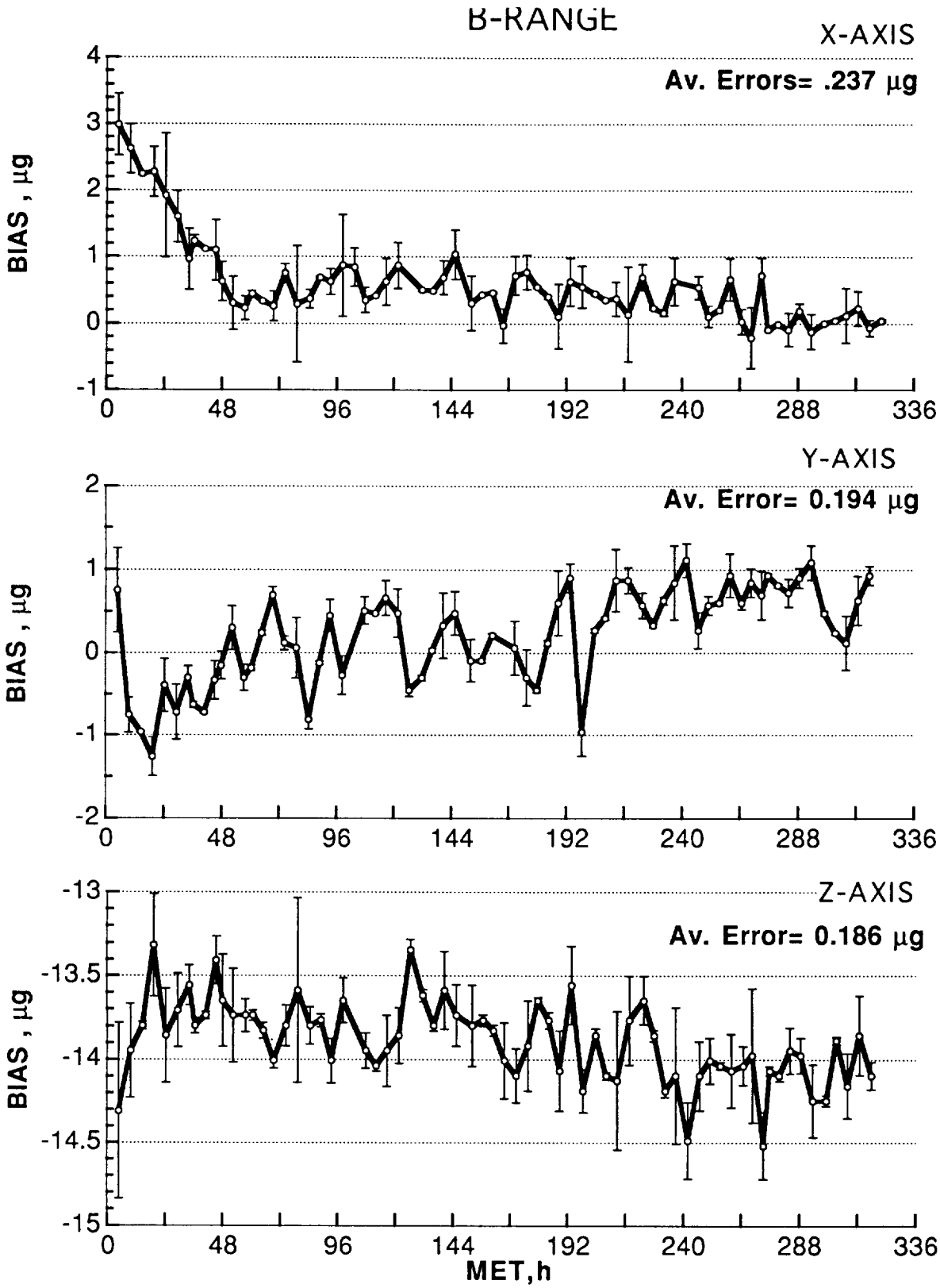

Fig. 9 OARE STS-58 B-range bias measurements with error bars.

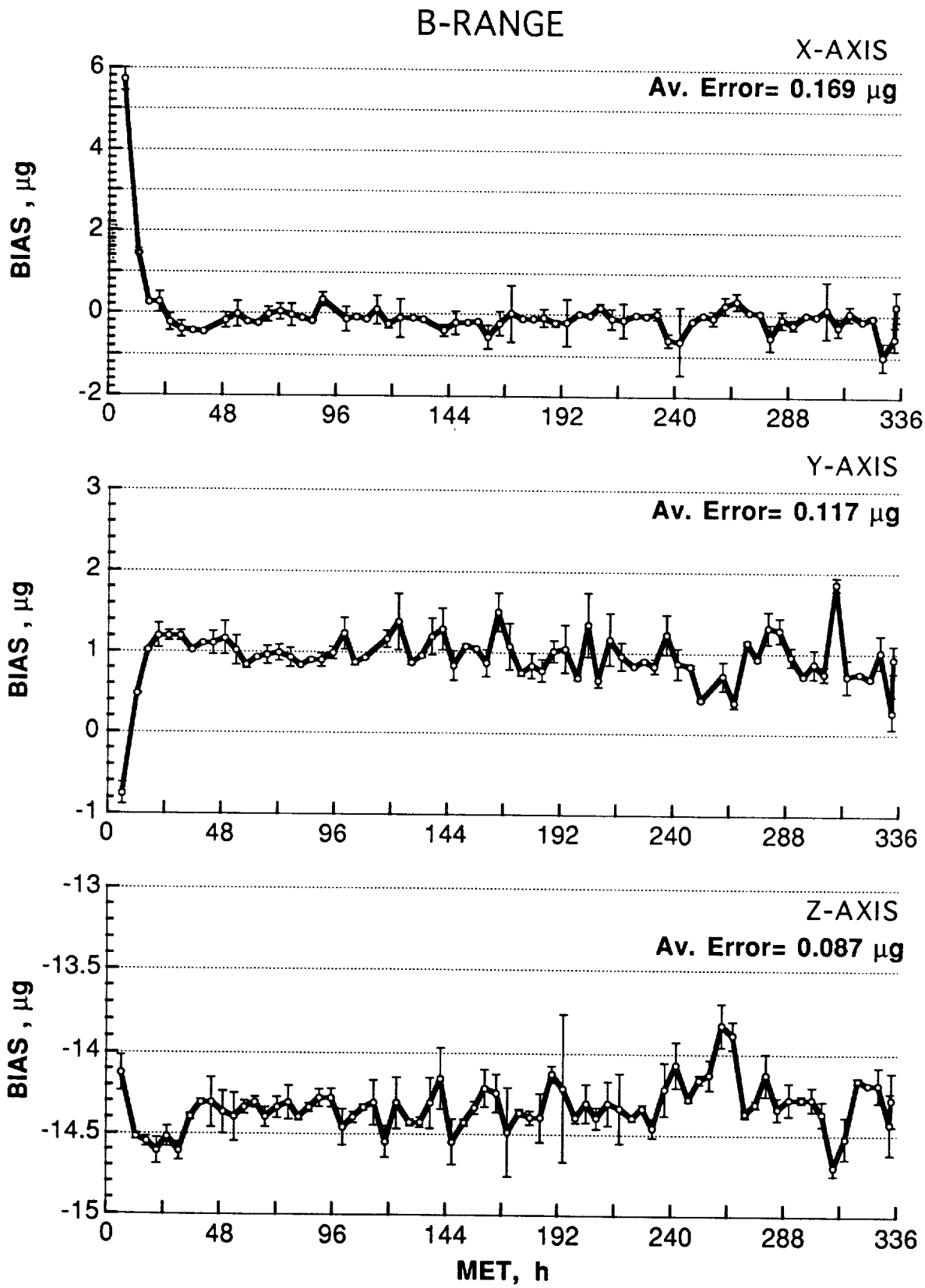

Fig. 10 OARE STS-62 B-range bias measurements with error bars.

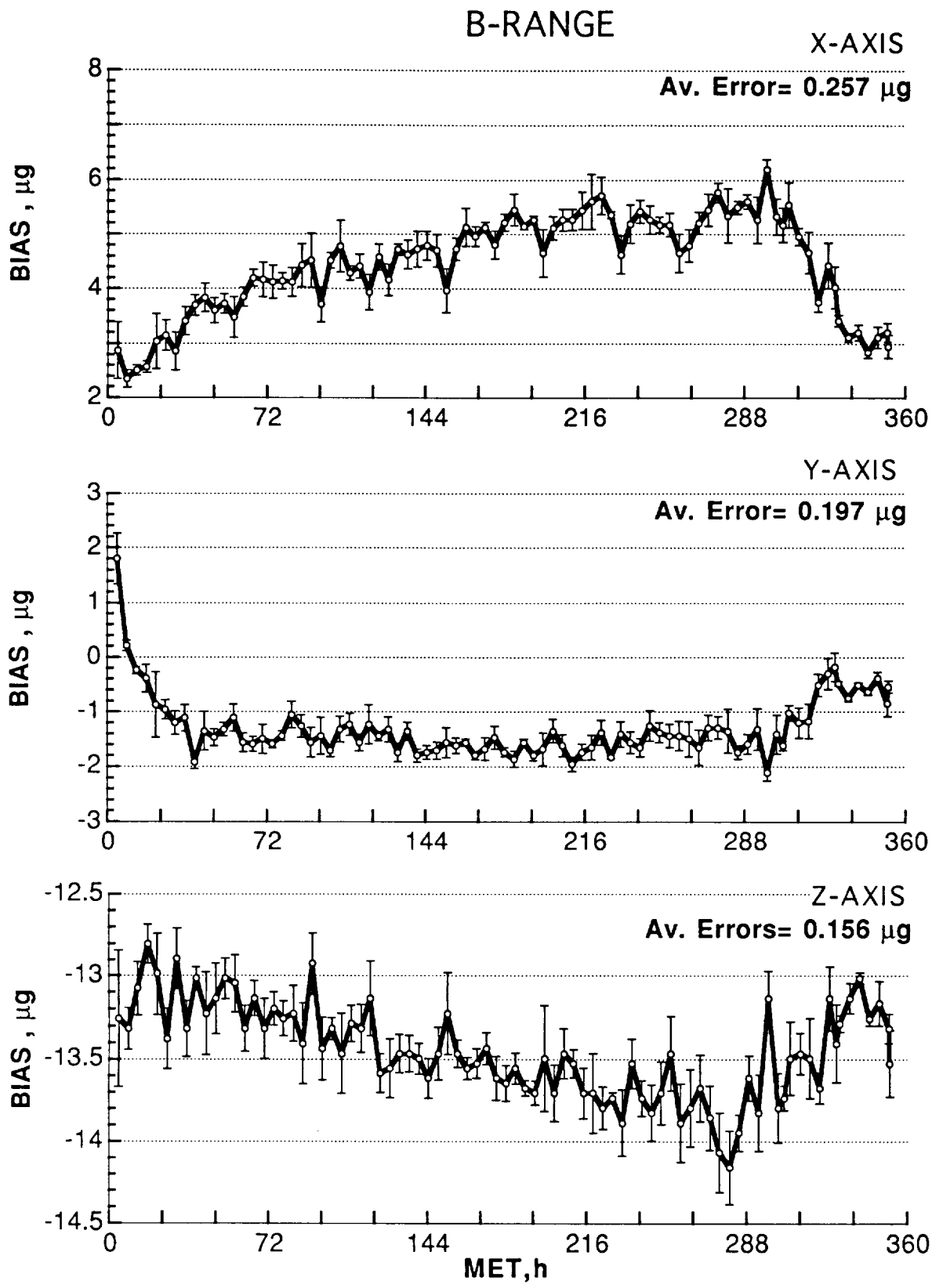

Fig. 11 OARE STS-65 B-range bias measurements with error bars.

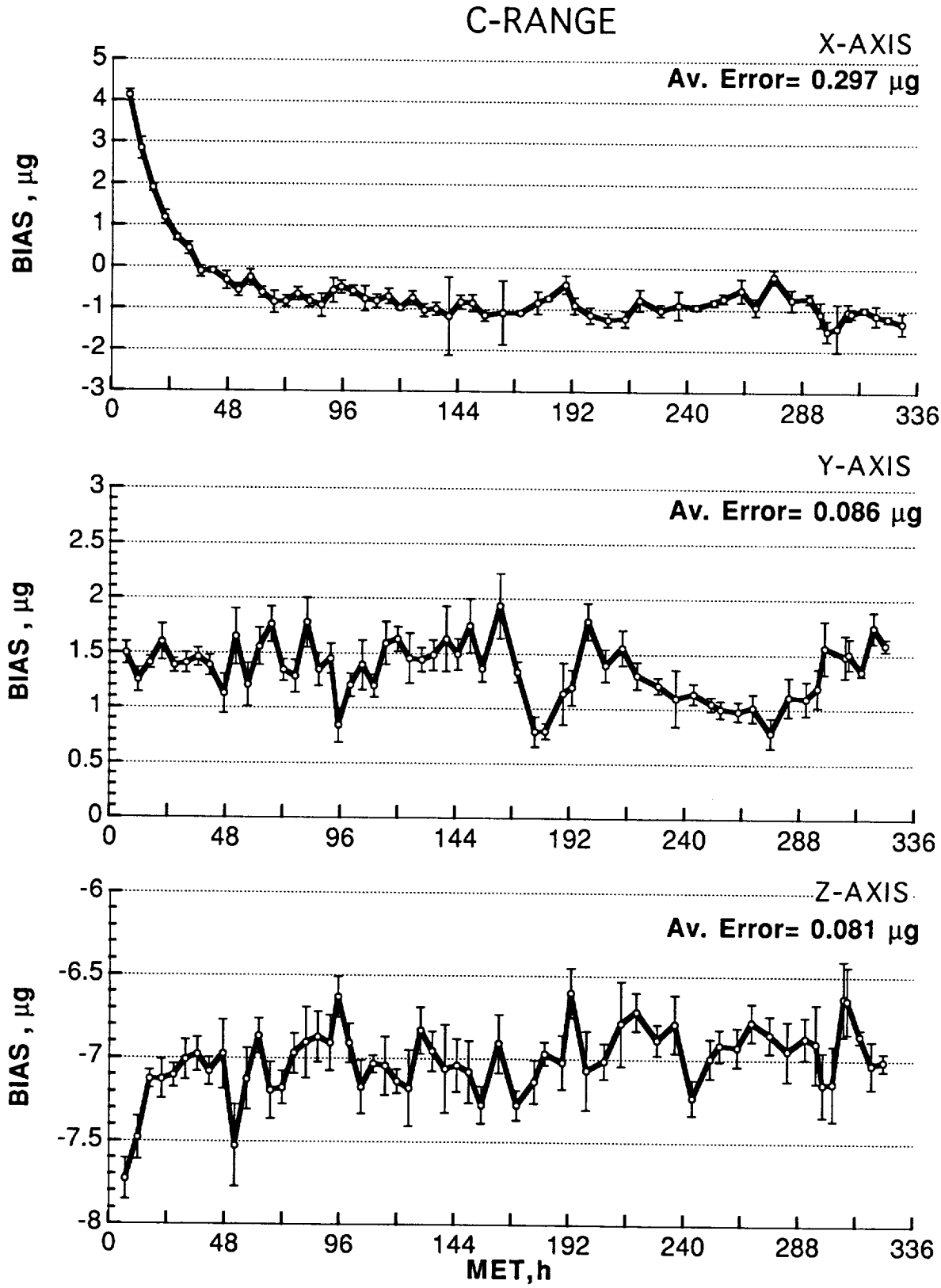

Fig. 12 OARE STS-50 C-range bias measurements with error bars.

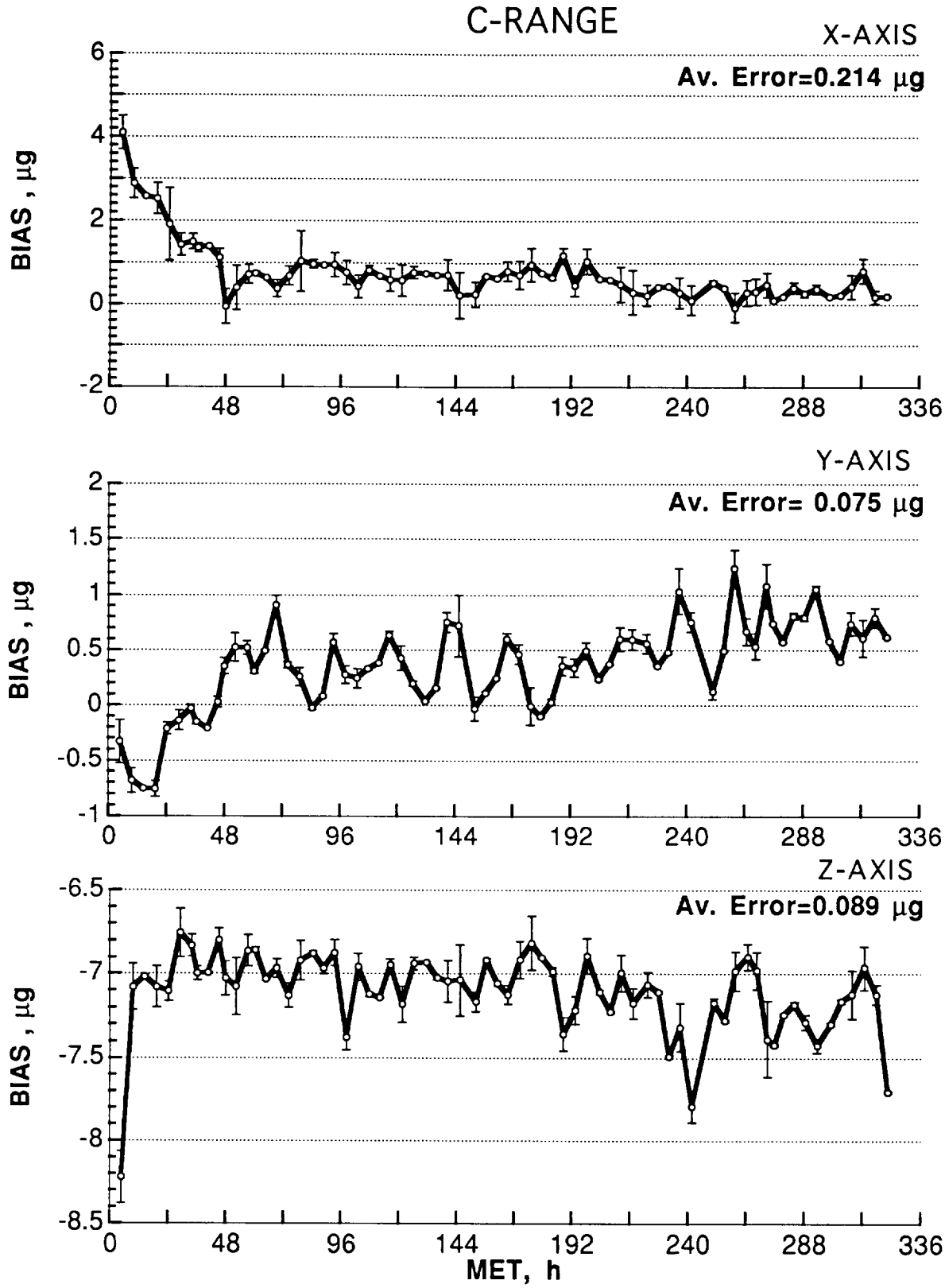

Fig. 13 OARE STS-58 C-Range bias measurements with error bars.

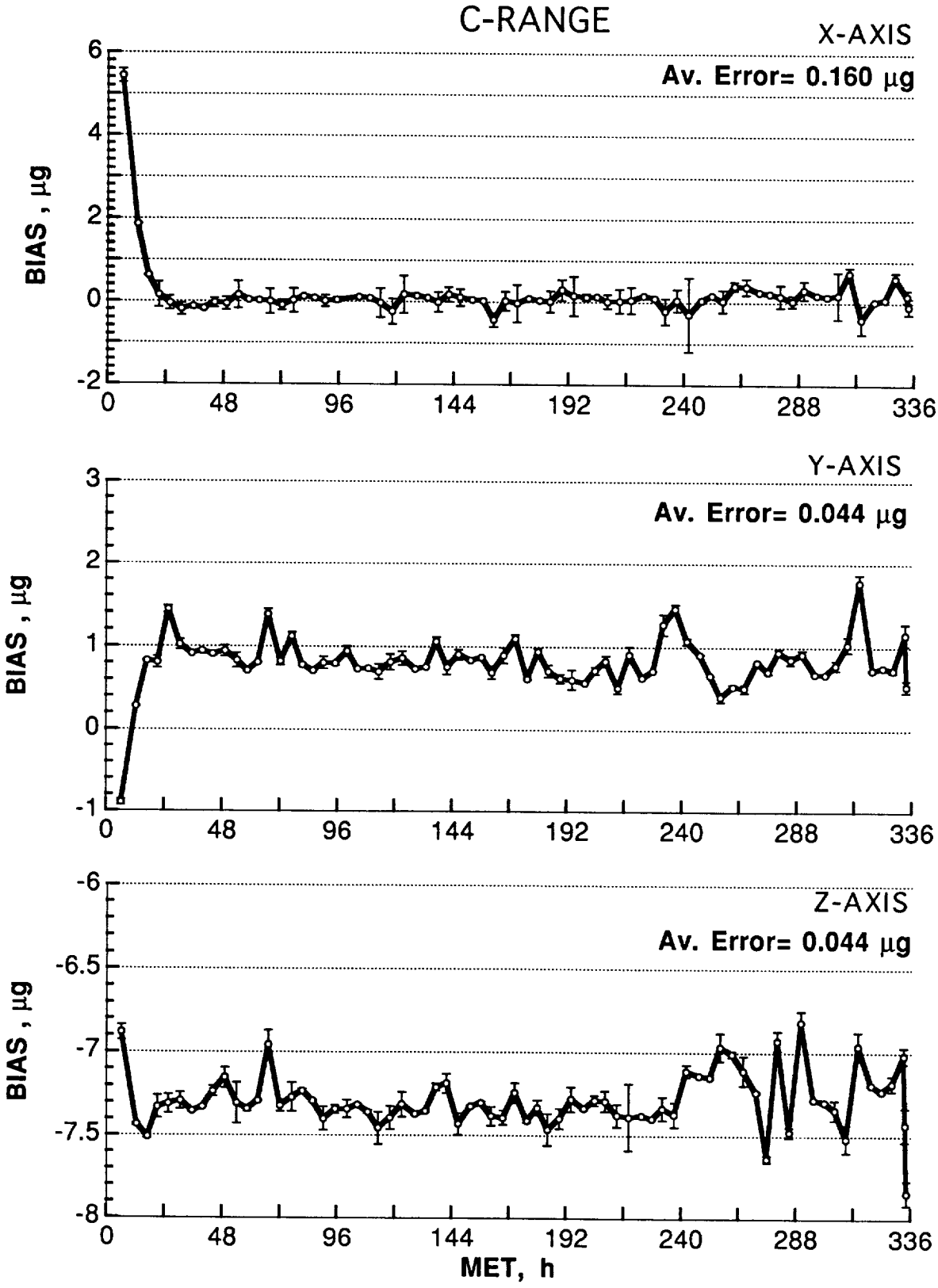

Fig. 14 OARE STS-62 C-Range bias measurements with error bars.

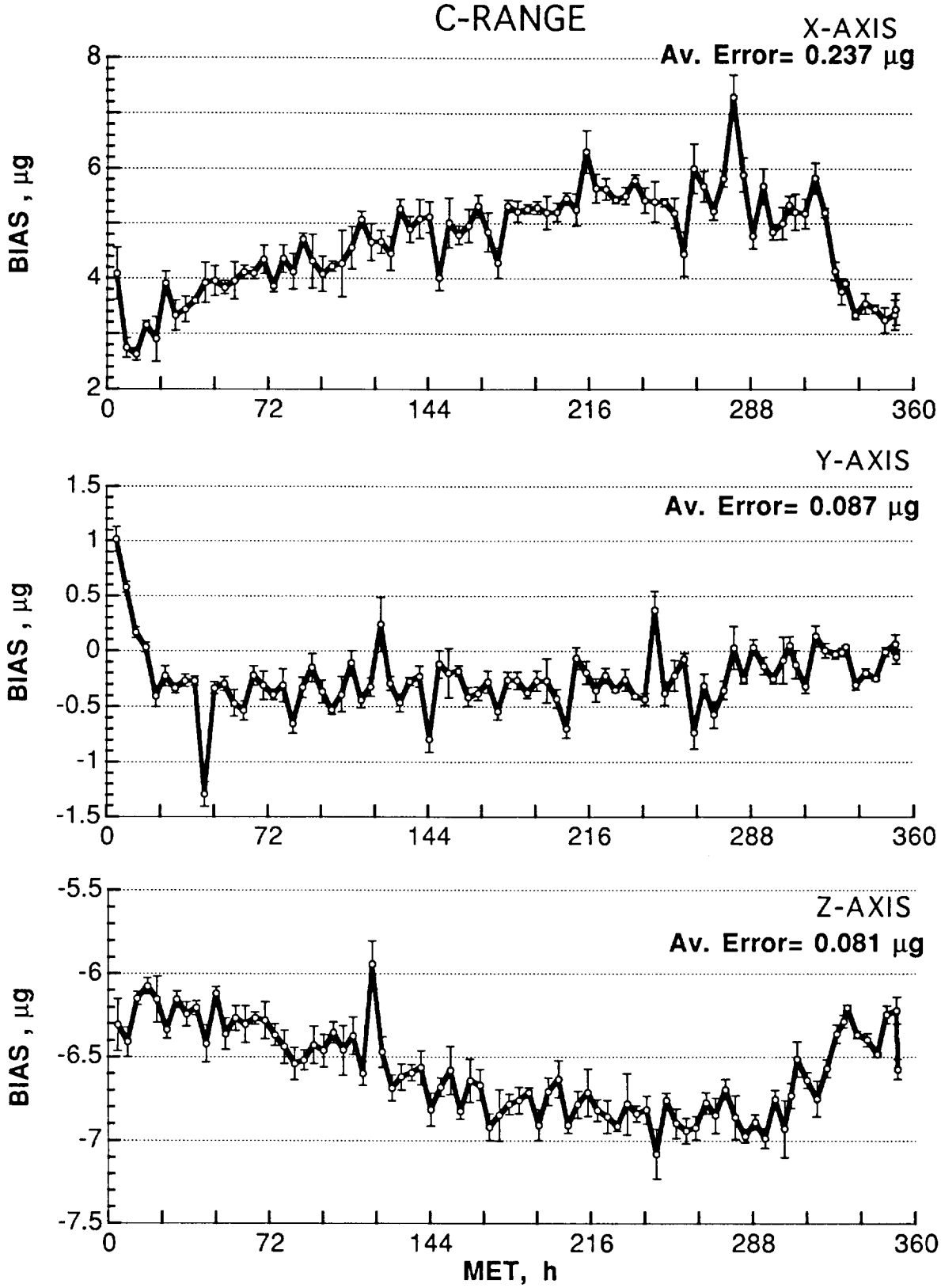

Fig. 15 OARE STS-65 C-range bias measurements with error bars.

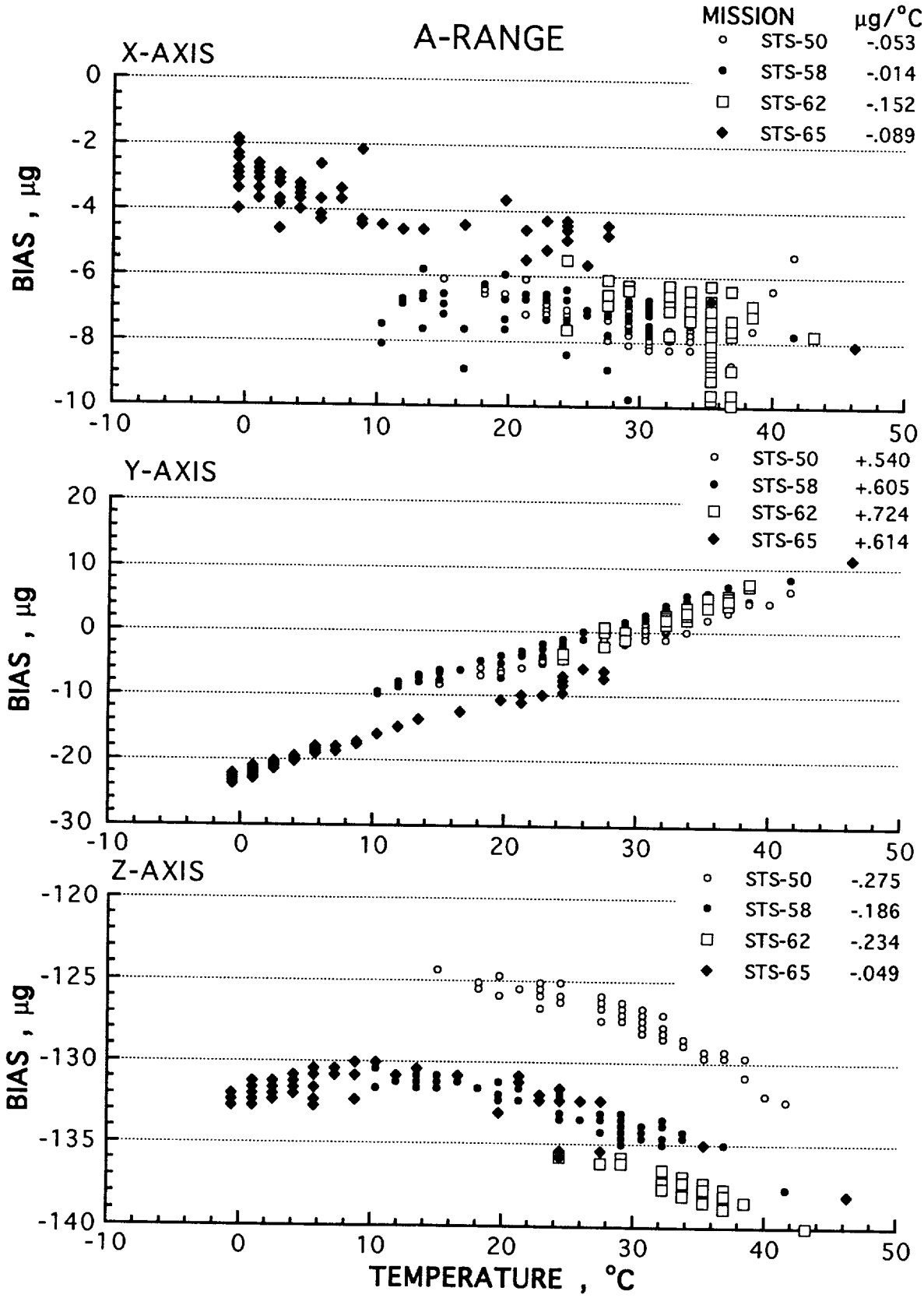

Fig. 16 In-flight bias temperature sensitivity measurements (A-Range).

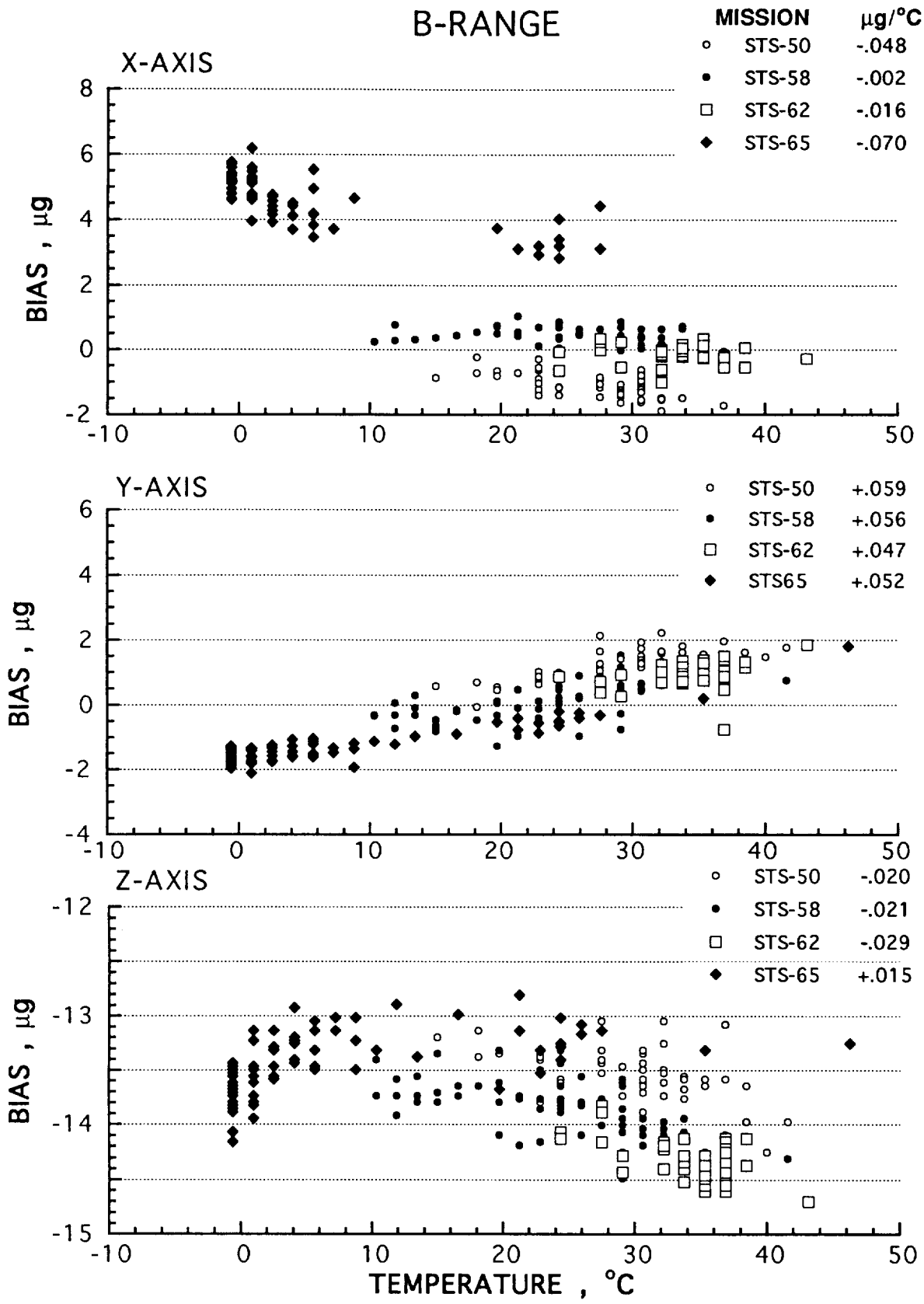

Fig. 17 In-flight bias temperature sensitivity measurements (B-Range).

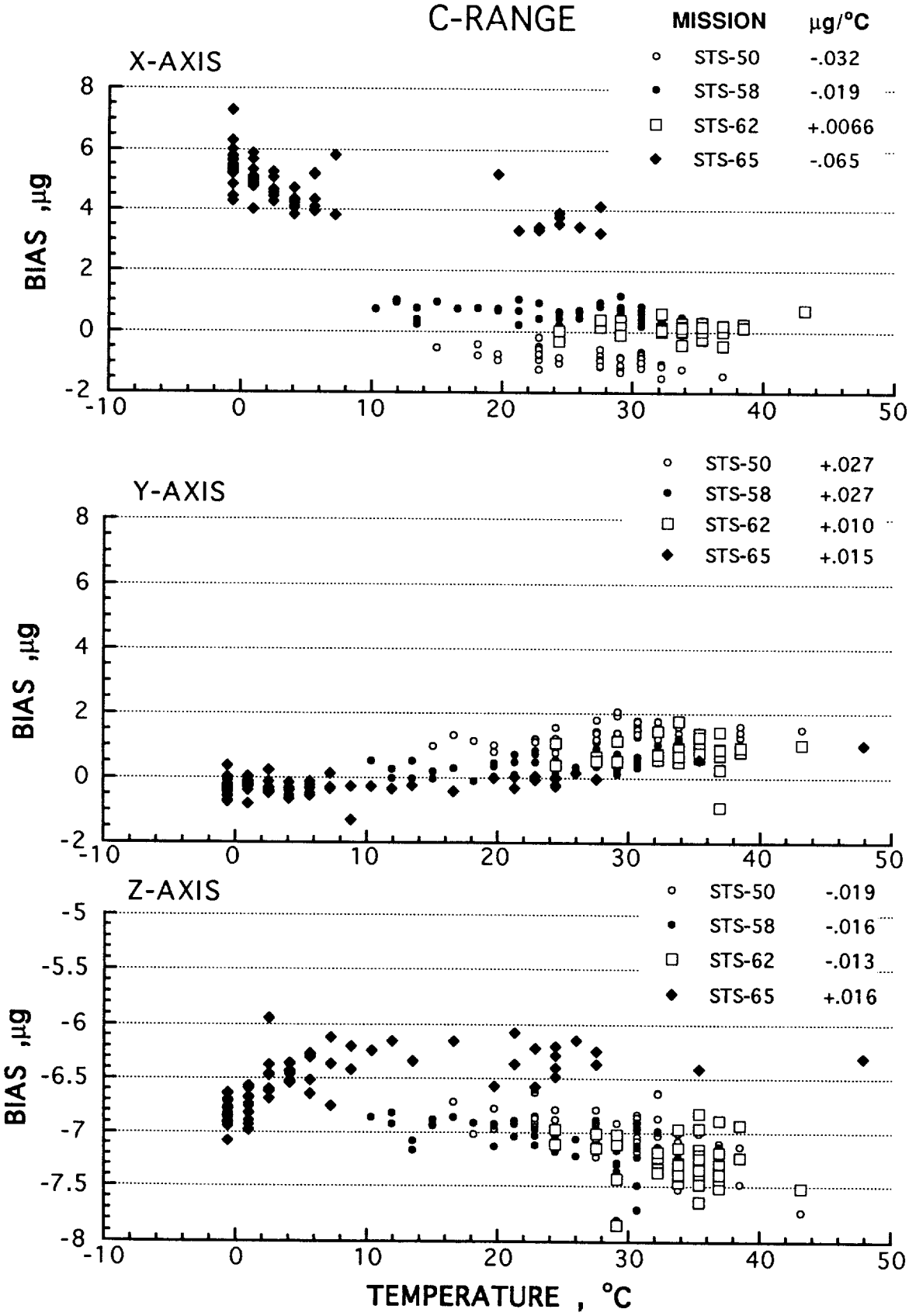

Fig. 18 In-flight bias temperature sensitivity measurements (C-Range).

SCALE FACTOR MEASUREMENT INDEX

FIG.	RANGE	MISSION	AXES*
19	A	STS-50	X,Y,Z
20		-58	"
21		-62	"
22		-65	"
23	B	STS-50	X,Y,Z
24		-58	"
25		-62	"
26		-65	"
27	C	STS-50	X,Y,Z
28		-58	"
29		-62	"
30		-65	"

*Two table directions and two rates for each axis

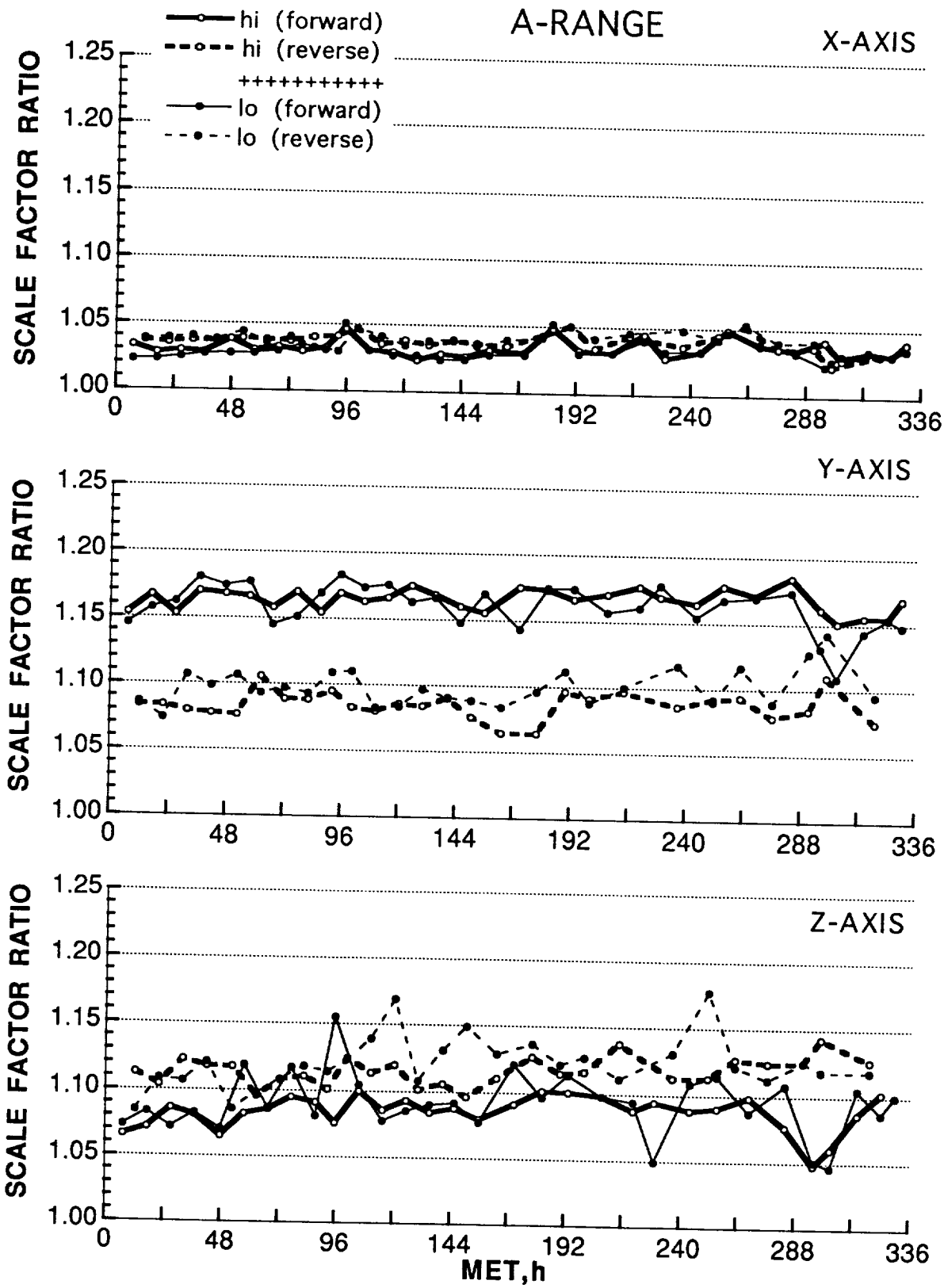

Fig. 19 OARE STS-50 scale factor measurements (A-Range).

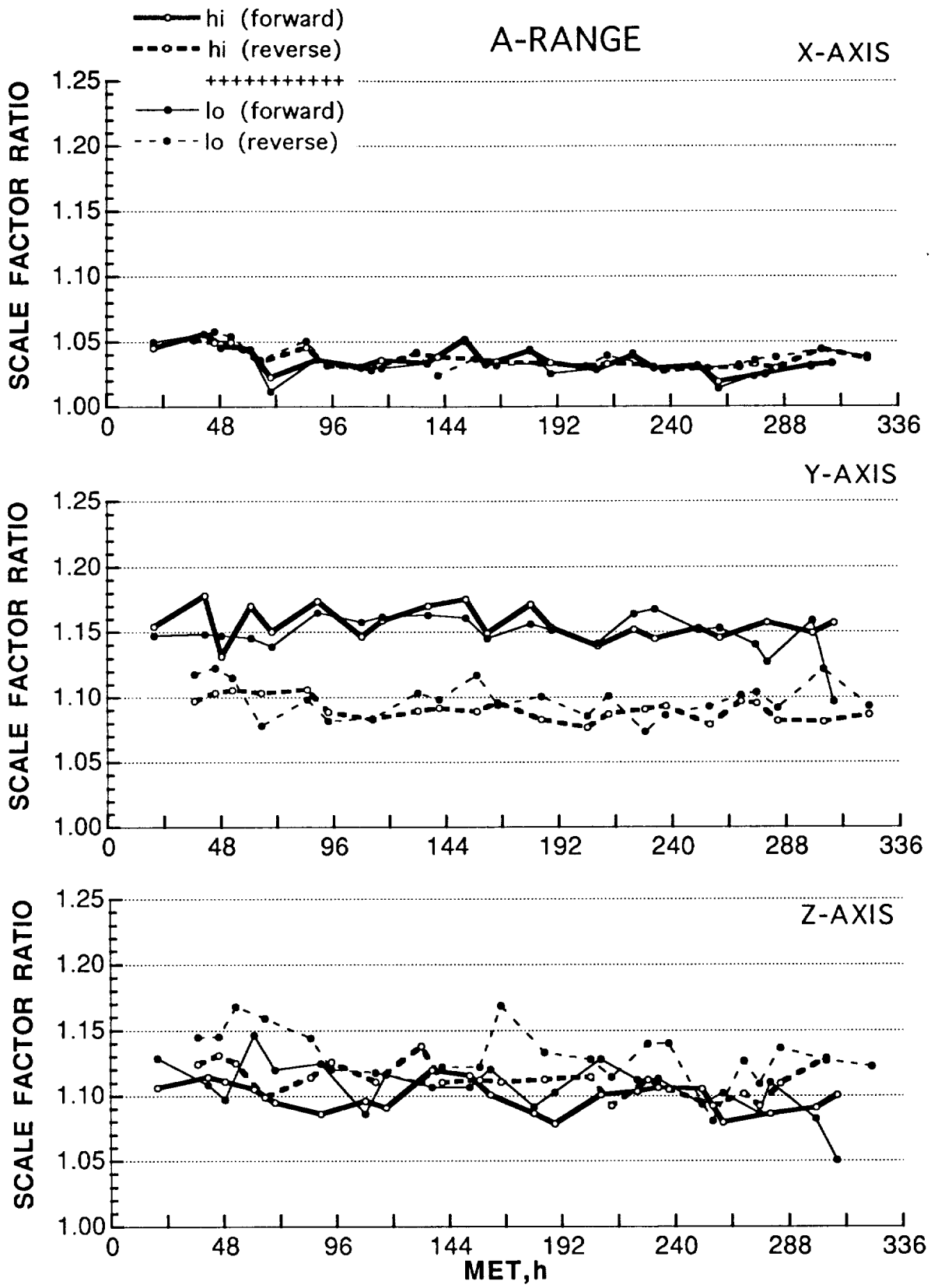

Fig. 20 OARE STS-58 scale factor measurements (A-Range).

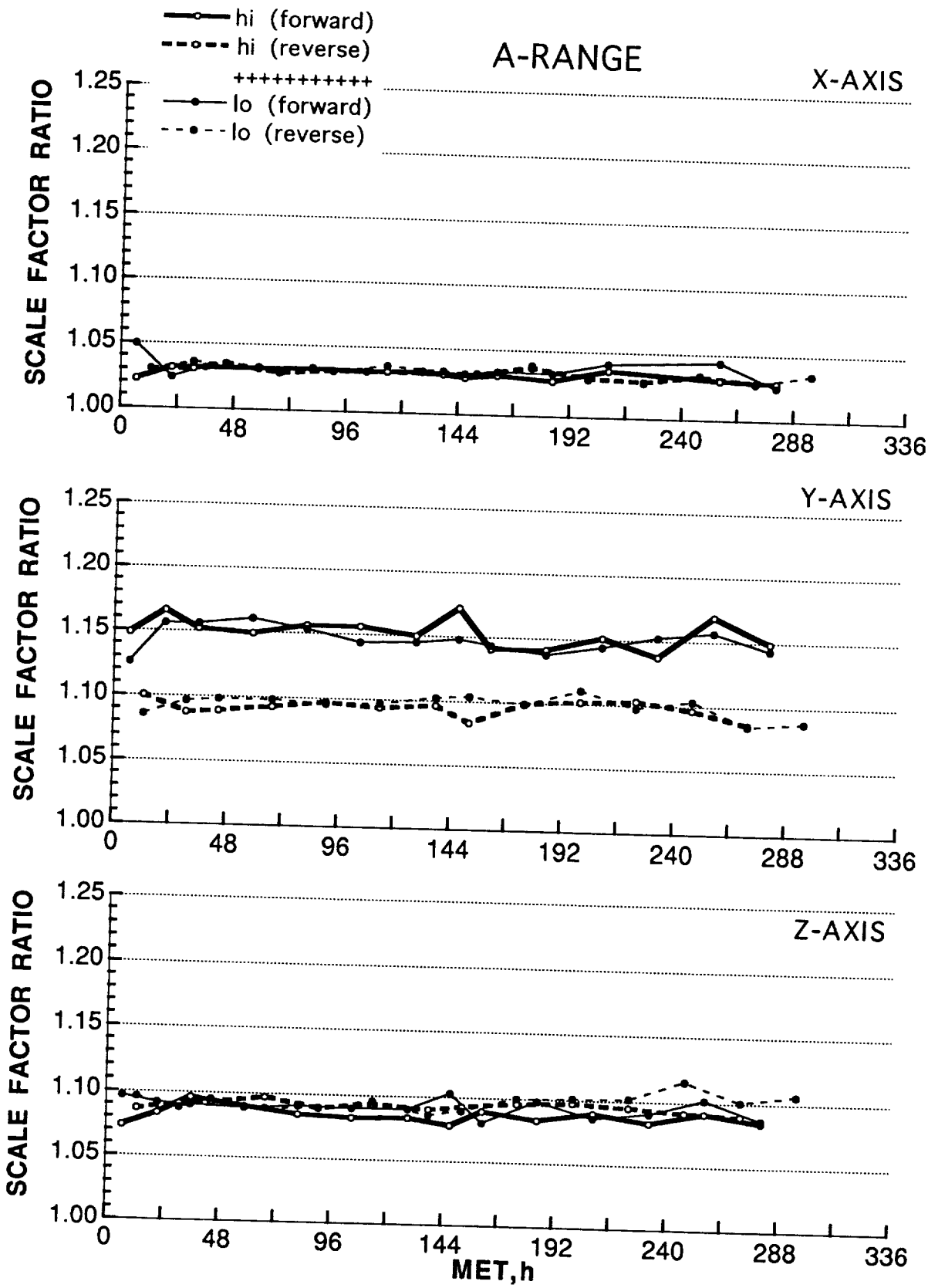

Fig. 21 OARE STS-62 scale factor measurements (A-Range).

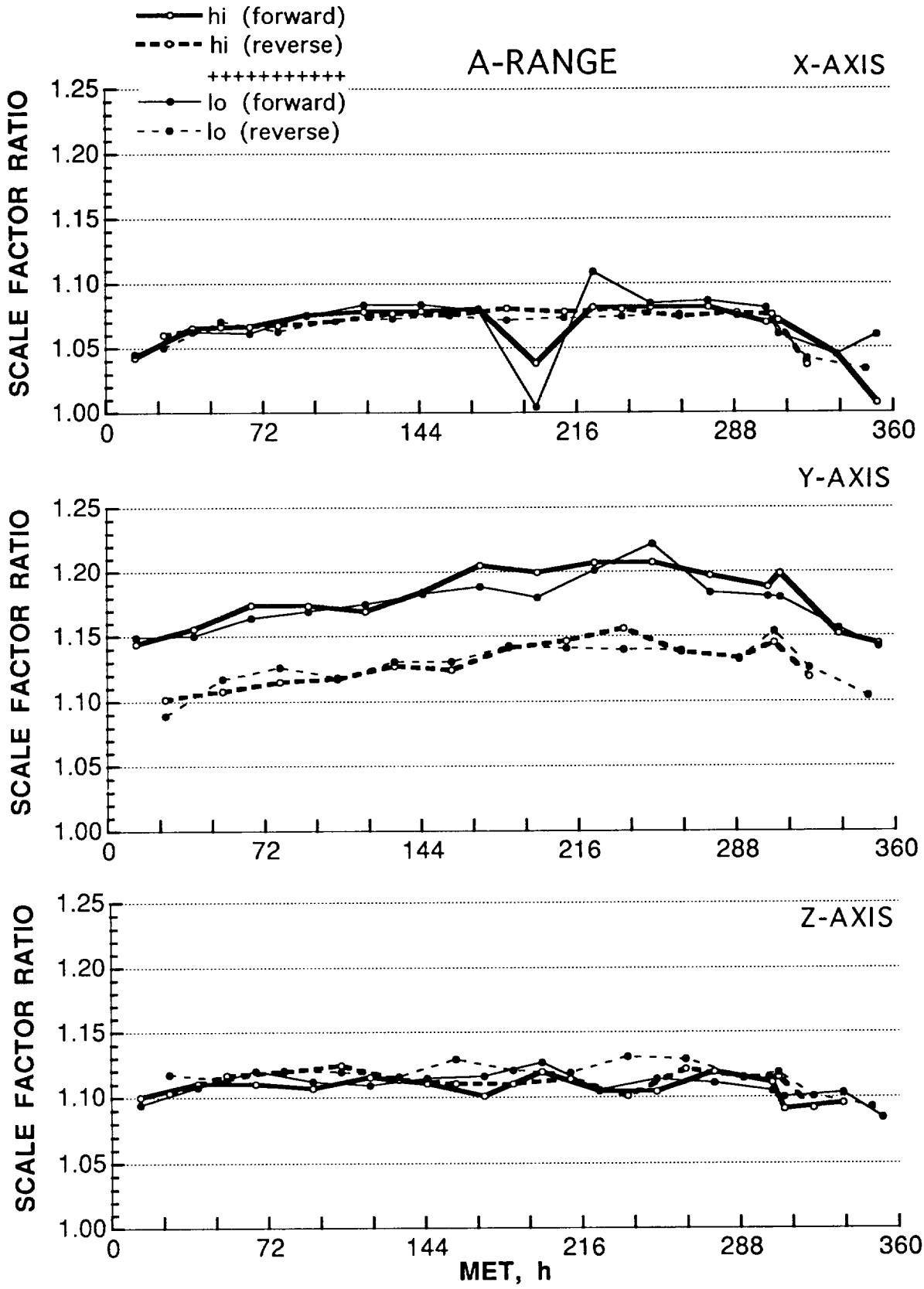

Fig. 22 OARE STS-65 scale factor measurements (A-Range).

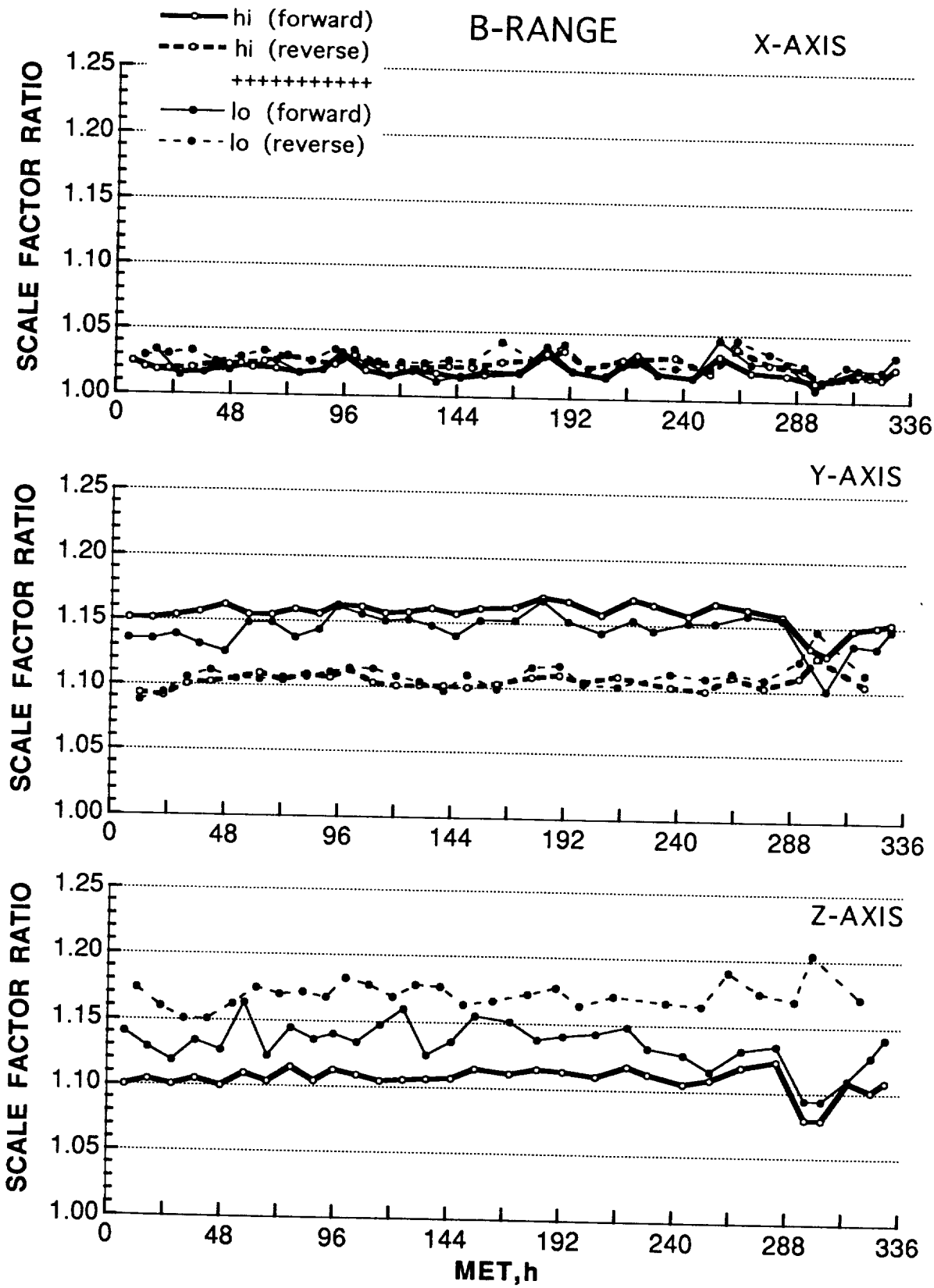

Fig. 23 OARE STS-50 scale factor measurements (B-Range).

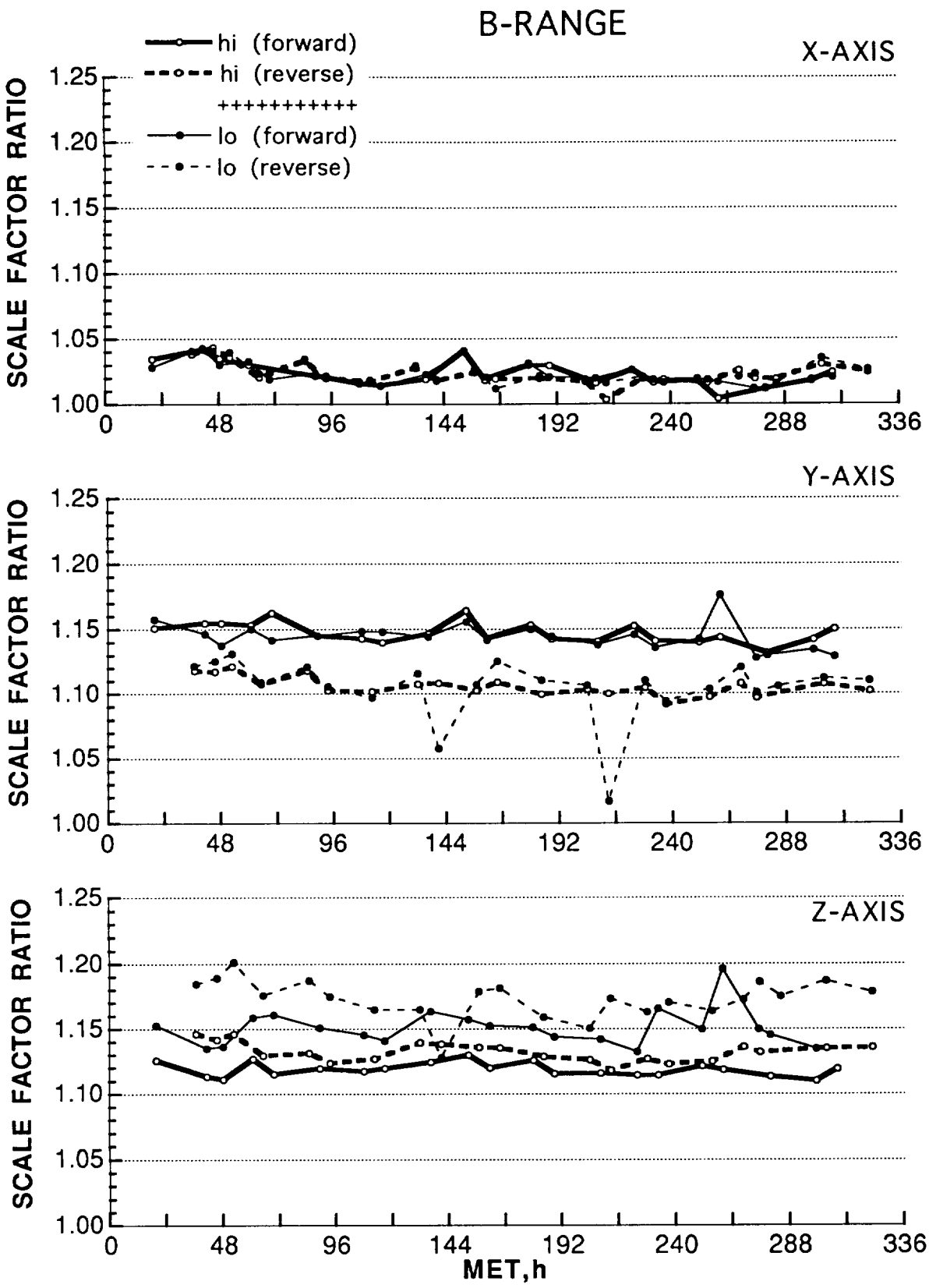

Fig. 24 OARE STS-58 scale factor measurements (B-Range).

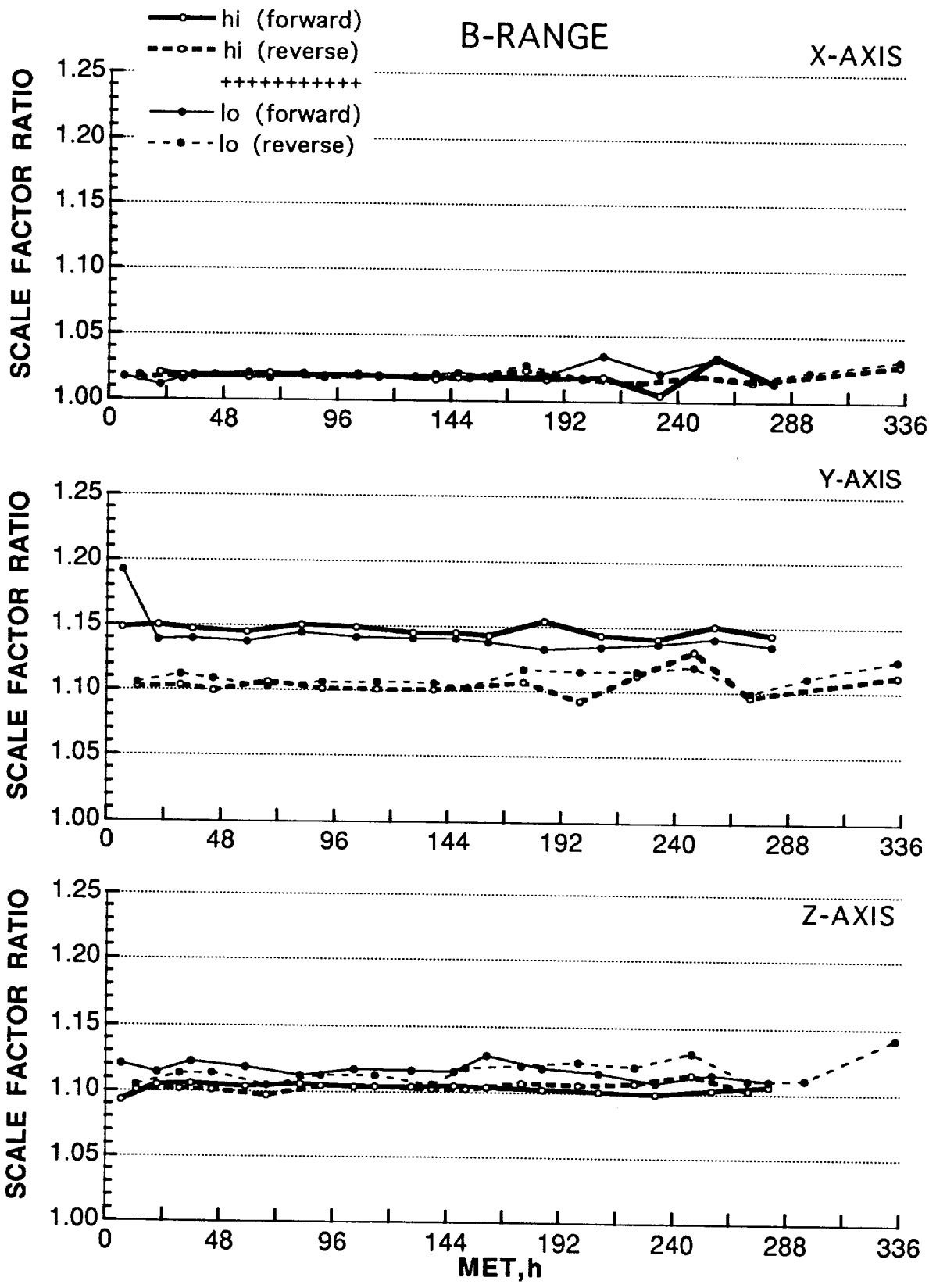

Fig. 25 OARE STS-62 scale factor measurements (B-Range).

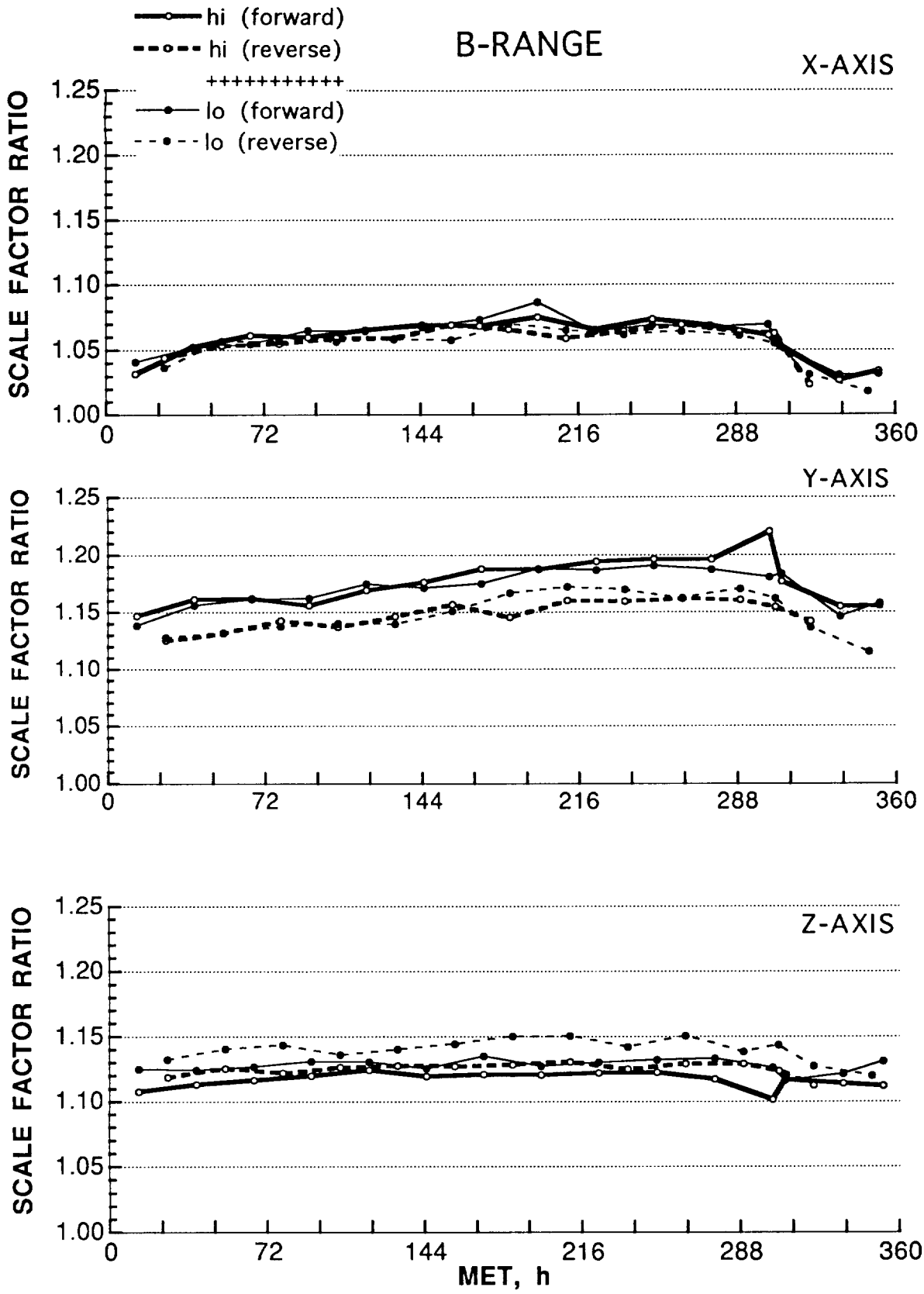

Fig. 26 OARE STS-65 scale factor measurements (B-Range)

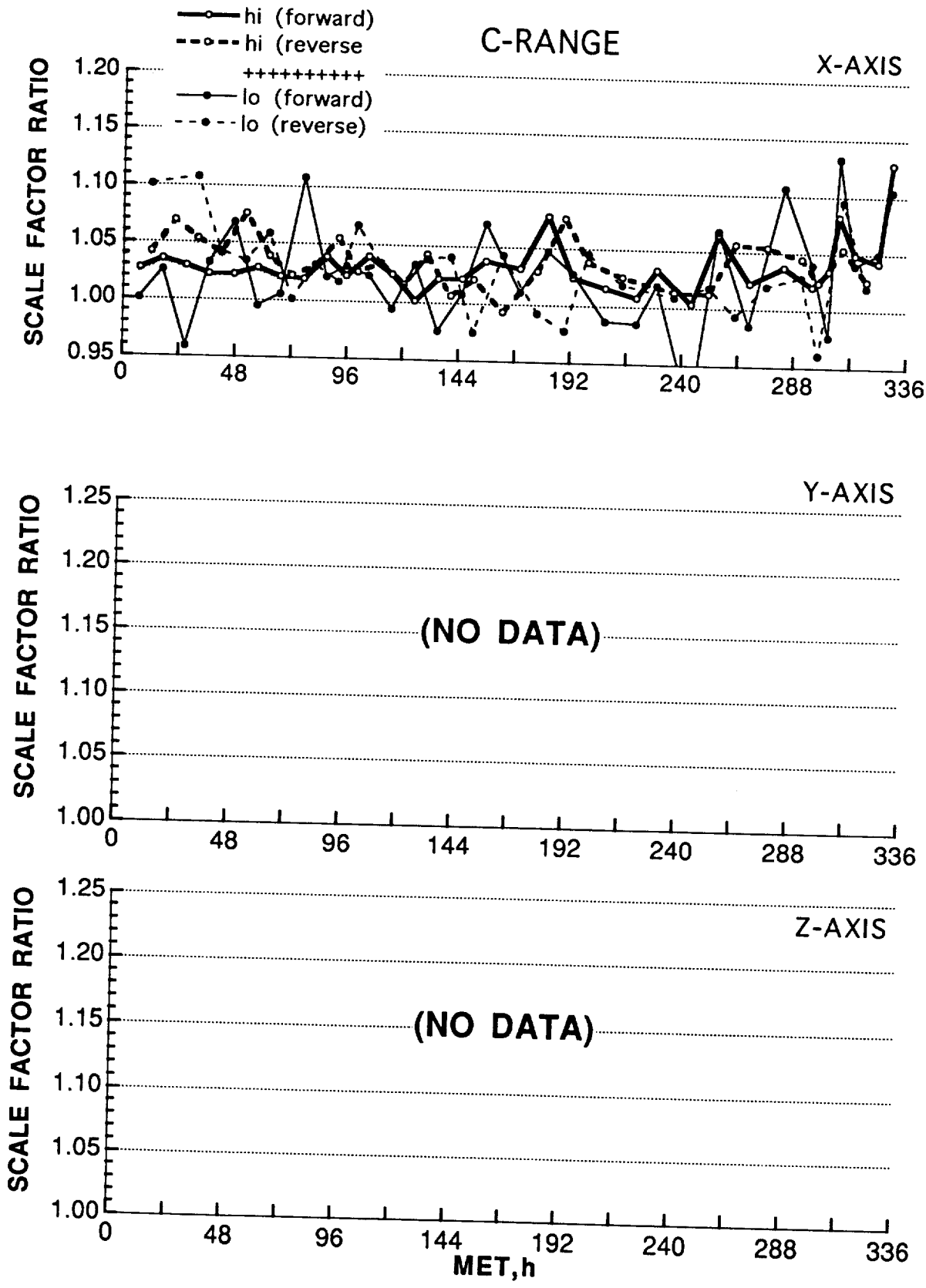

Fig. 27 OARE STS-50 scale factor measurements (C-Range).

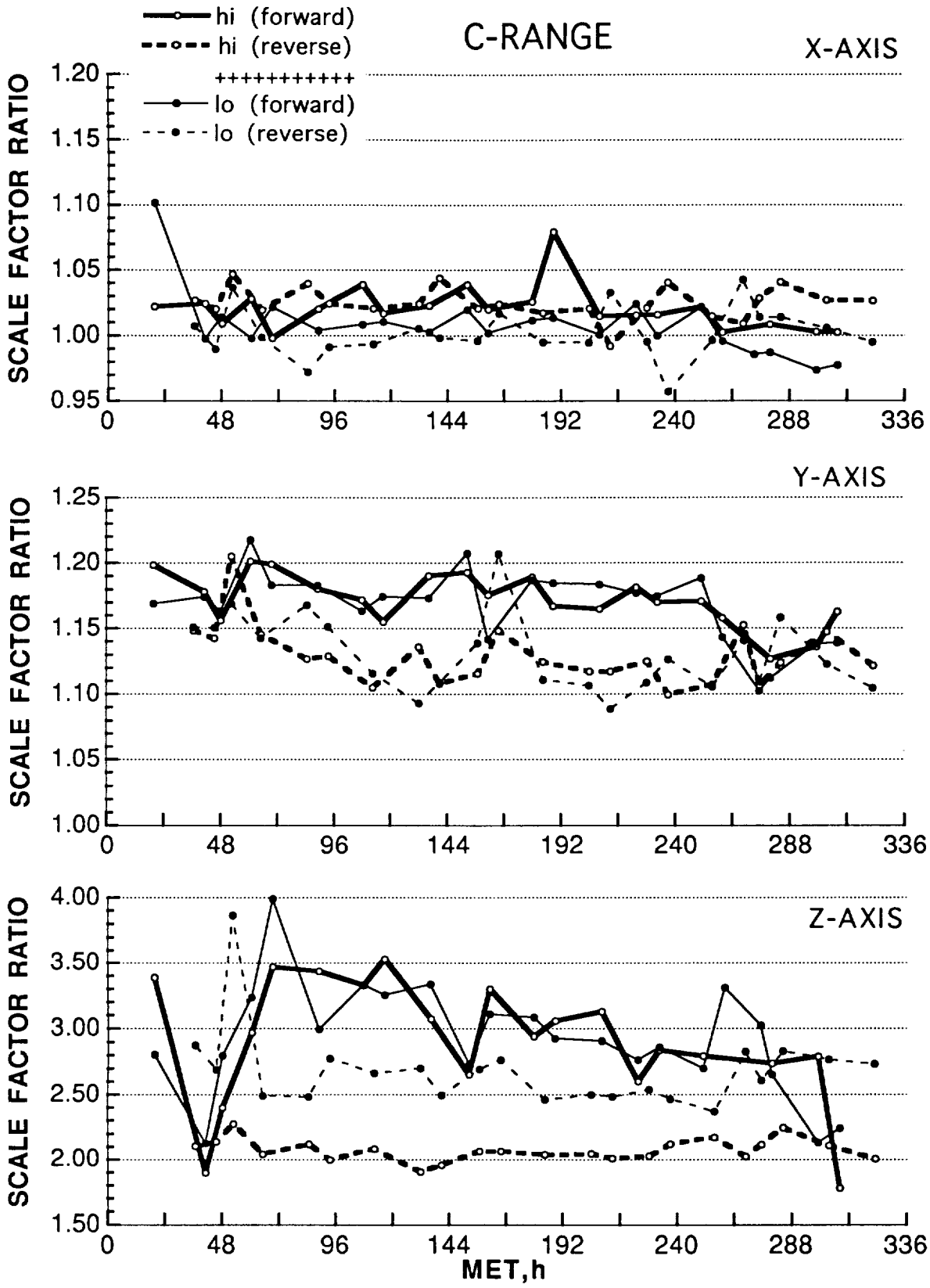

Fig. 28 OARE STS-58 scale factor measurements (C-Range).

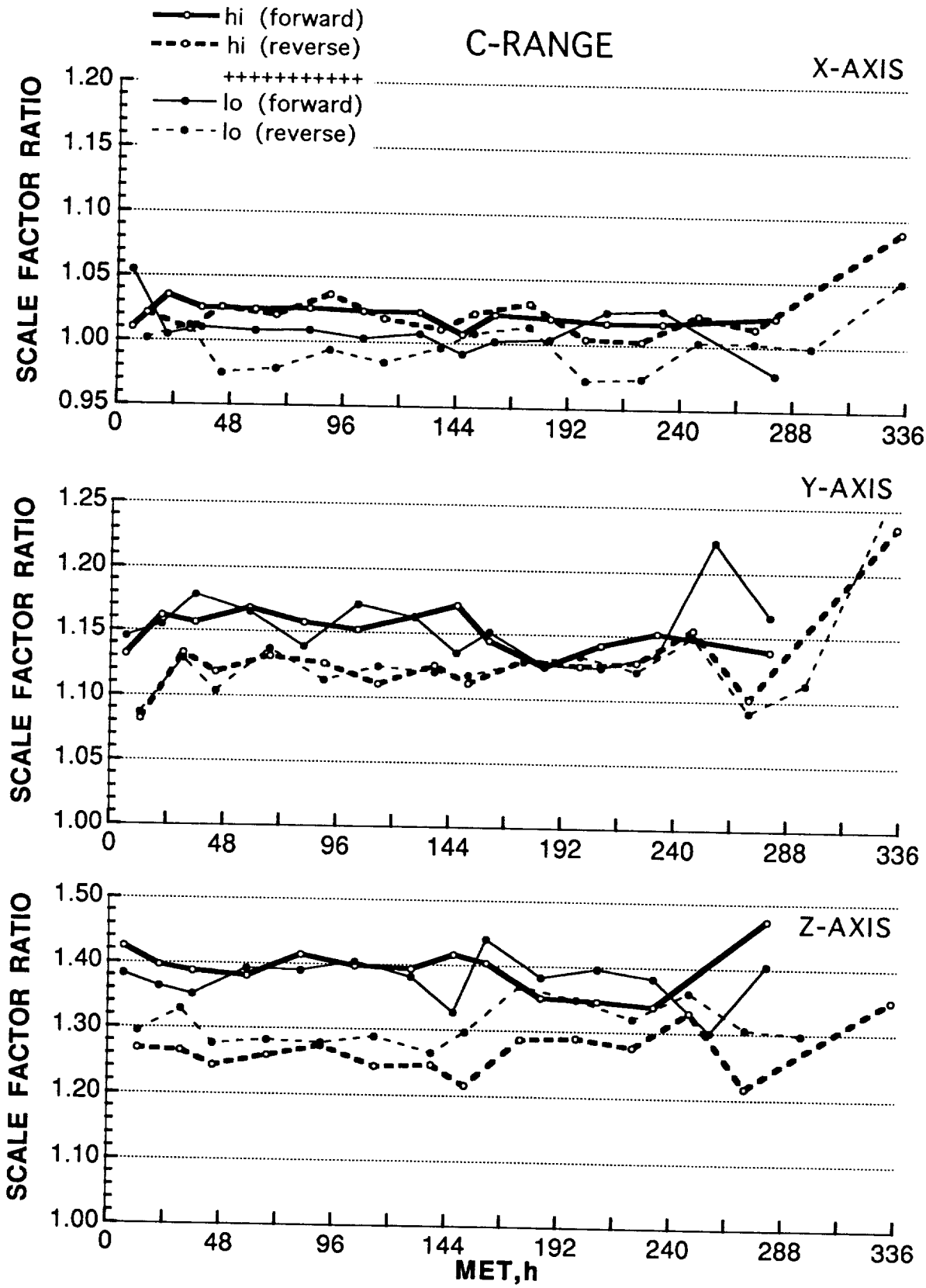

Fig. 29 OARE STS-62 scale factor measurements (C-Range).

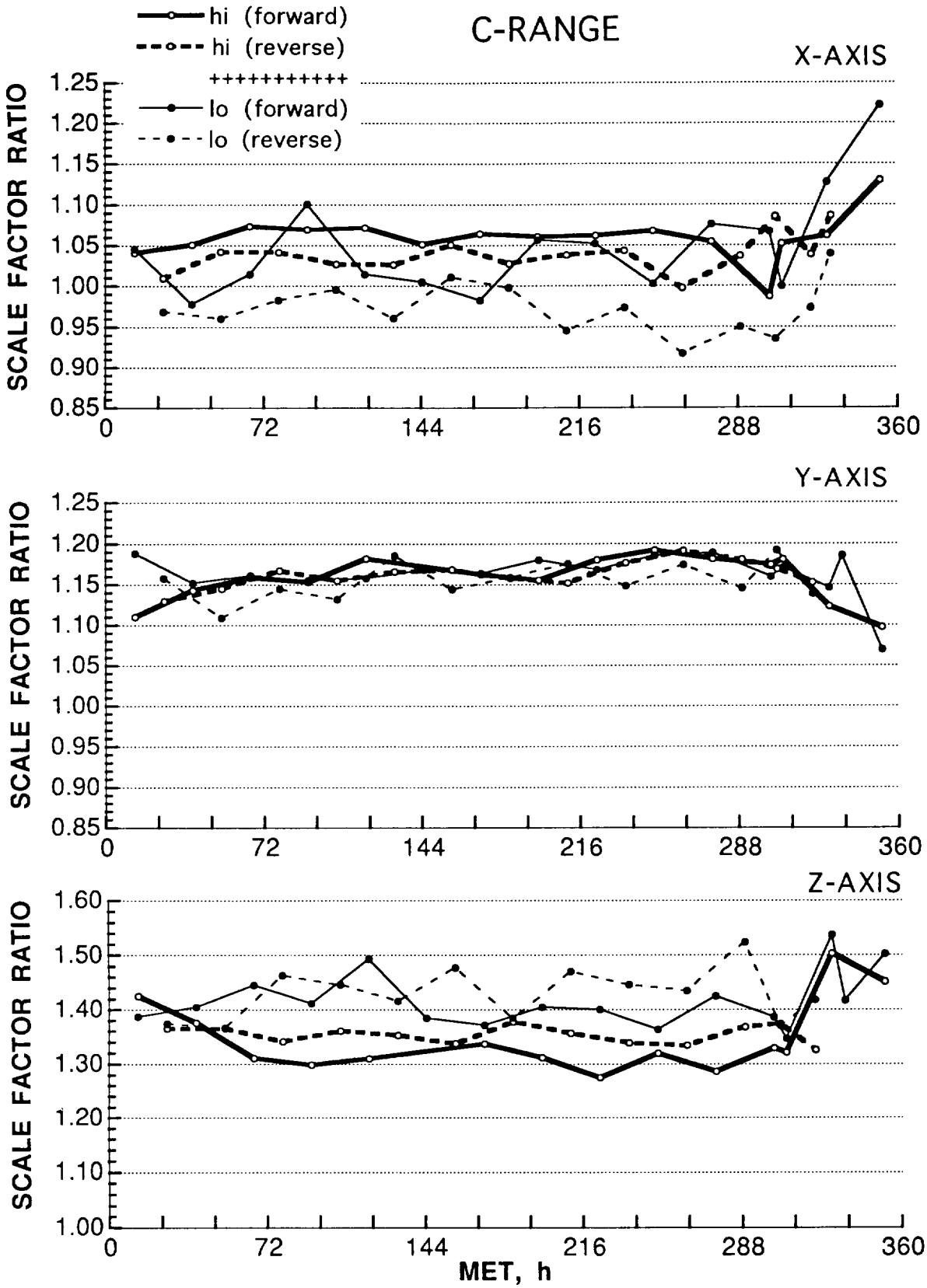

Fig. 30 OARE STS-65 scale factor measurements (C-Range).

SCALE FACTOR MEASUREMENT ERRORS INDEX

FIG.	RANGE	MISSION	AXES*
31	A	STS-50	X,Y,Z
32		-58	"
33		-62	"
34		-65	"
35	B	STS-50	X,Y,Z
36		-58	"
37		-62	"
38		-65	"
39	C	STS-50	X,Y,Z
40		-58	"
41		-62	"
42		-65	"

*Two table directions and two rates for each axis

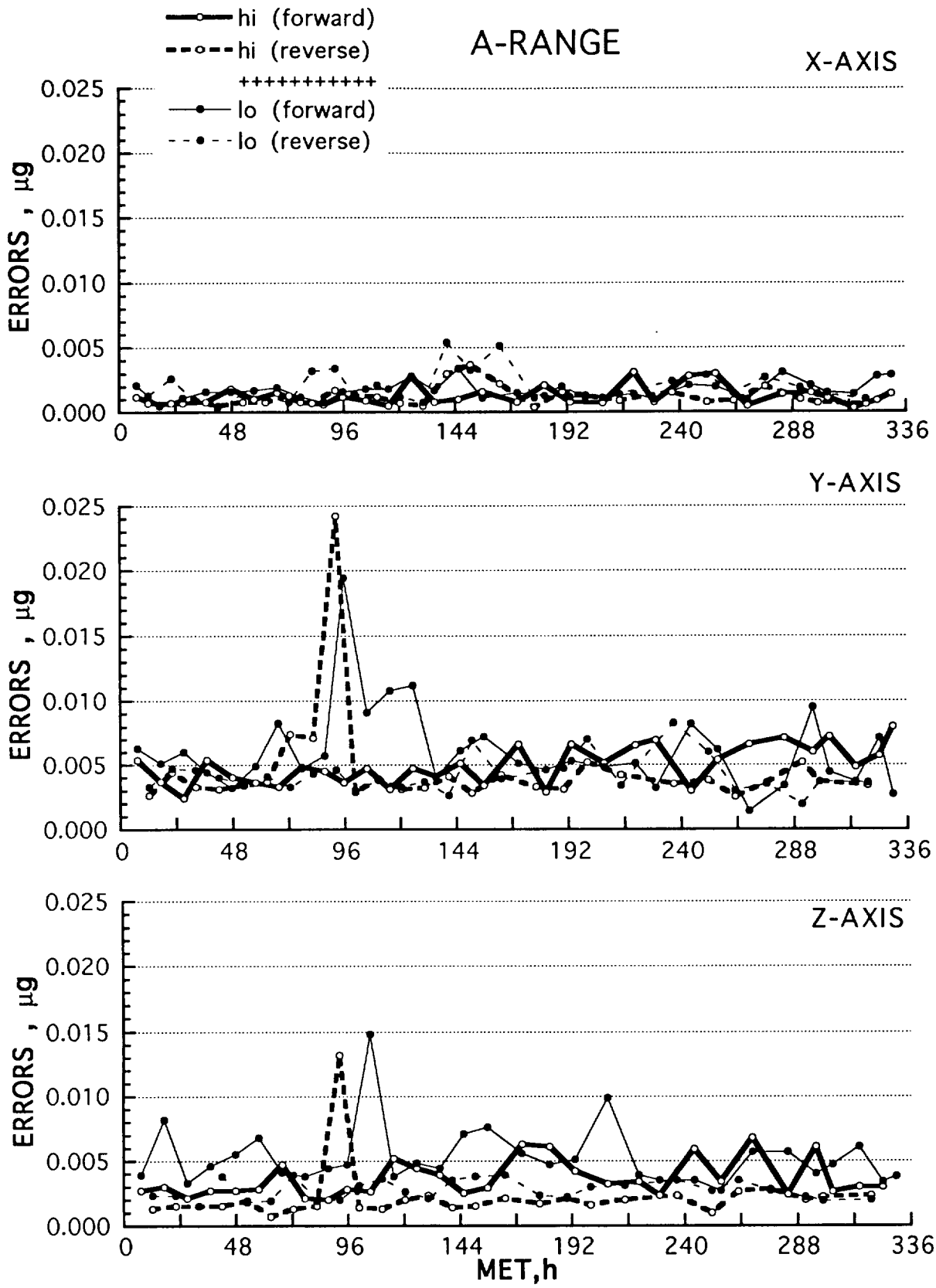

Fig. 31 OARE STS-50 scale factor measurement average errors (A-Range).

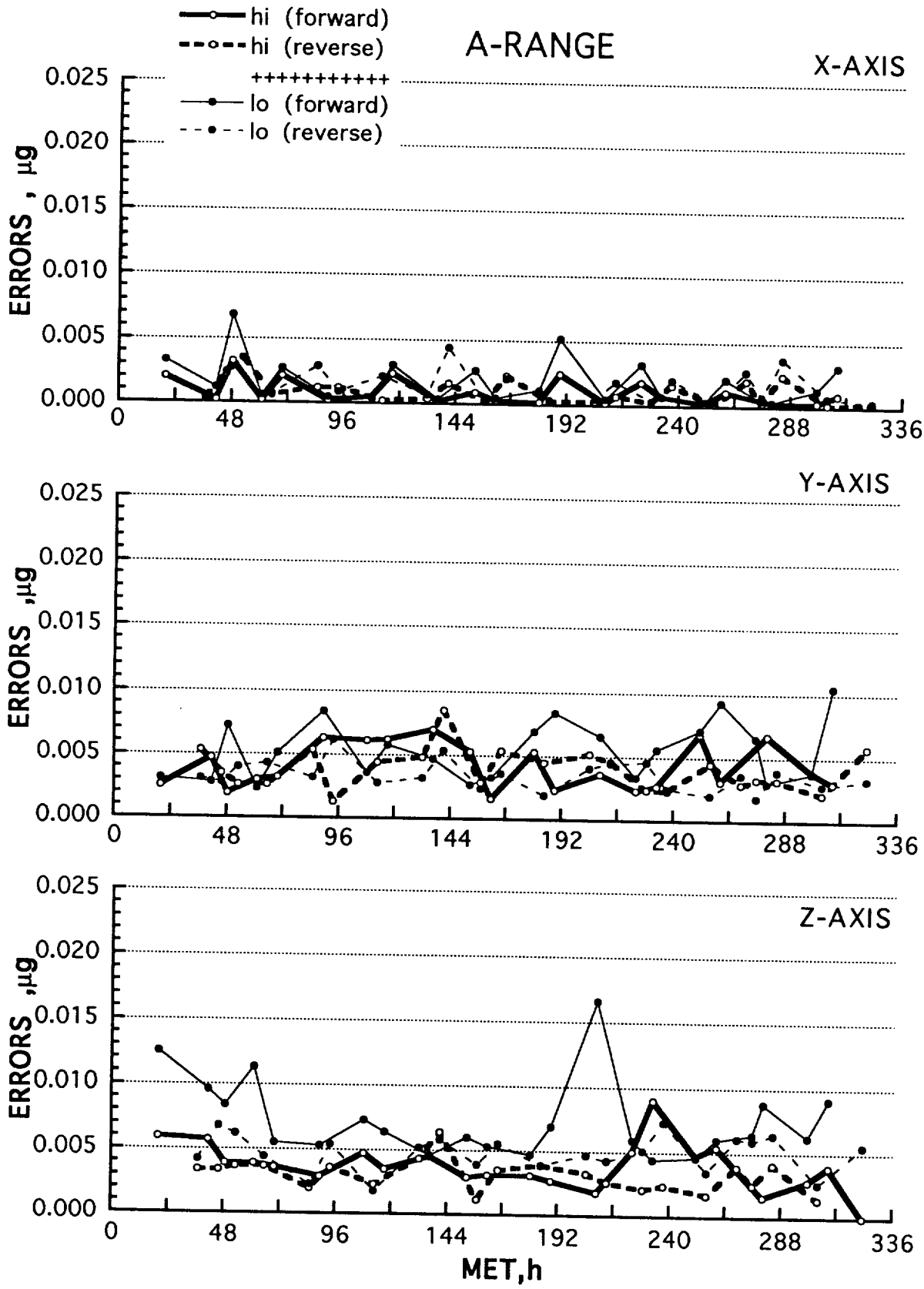

Fig. 32 OARE STS-58 scale factor measurement average errors (A-Range).

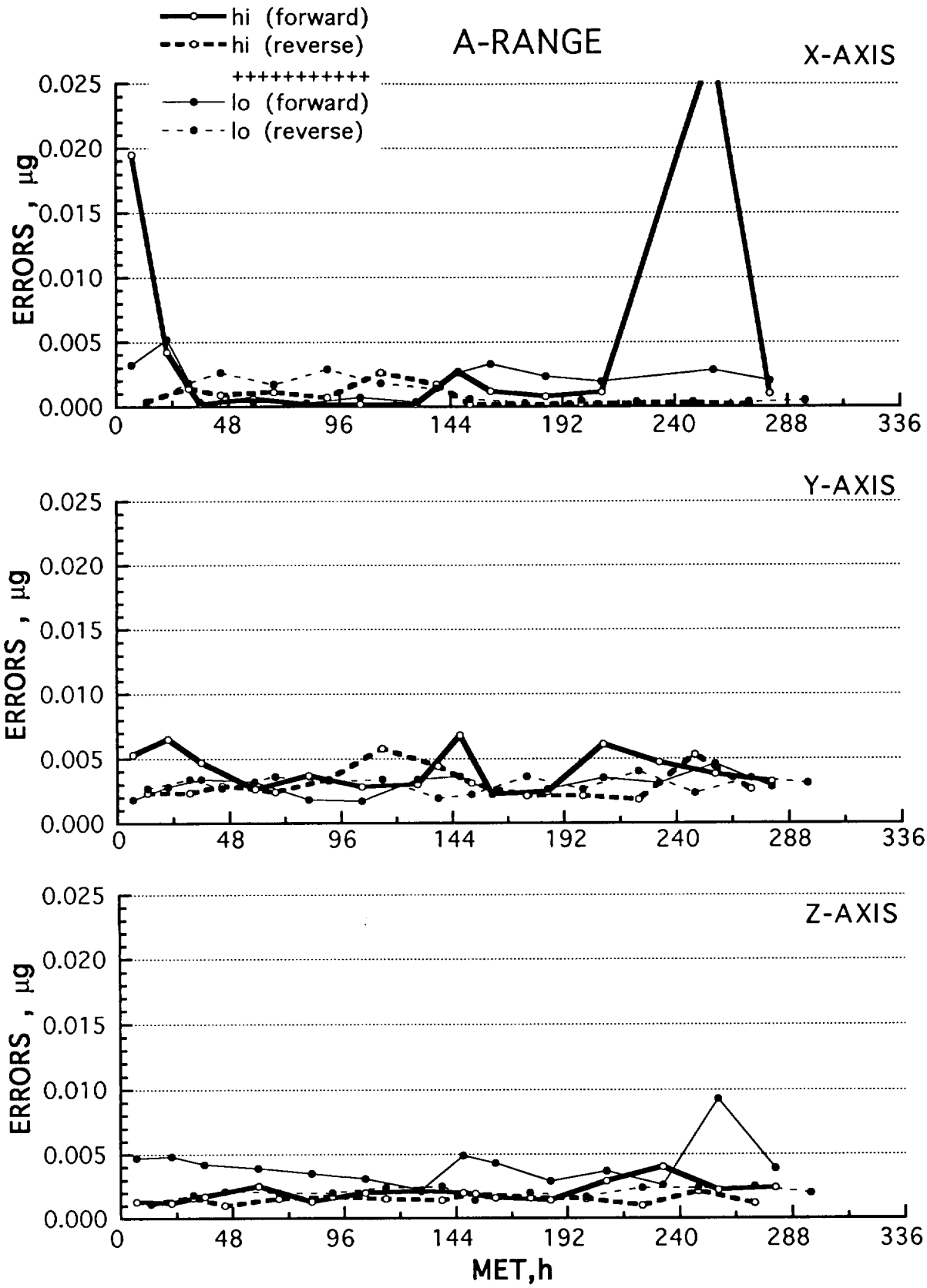

Fig. 33 OARE STS-62 scale factor measurement average errors (A-Range).

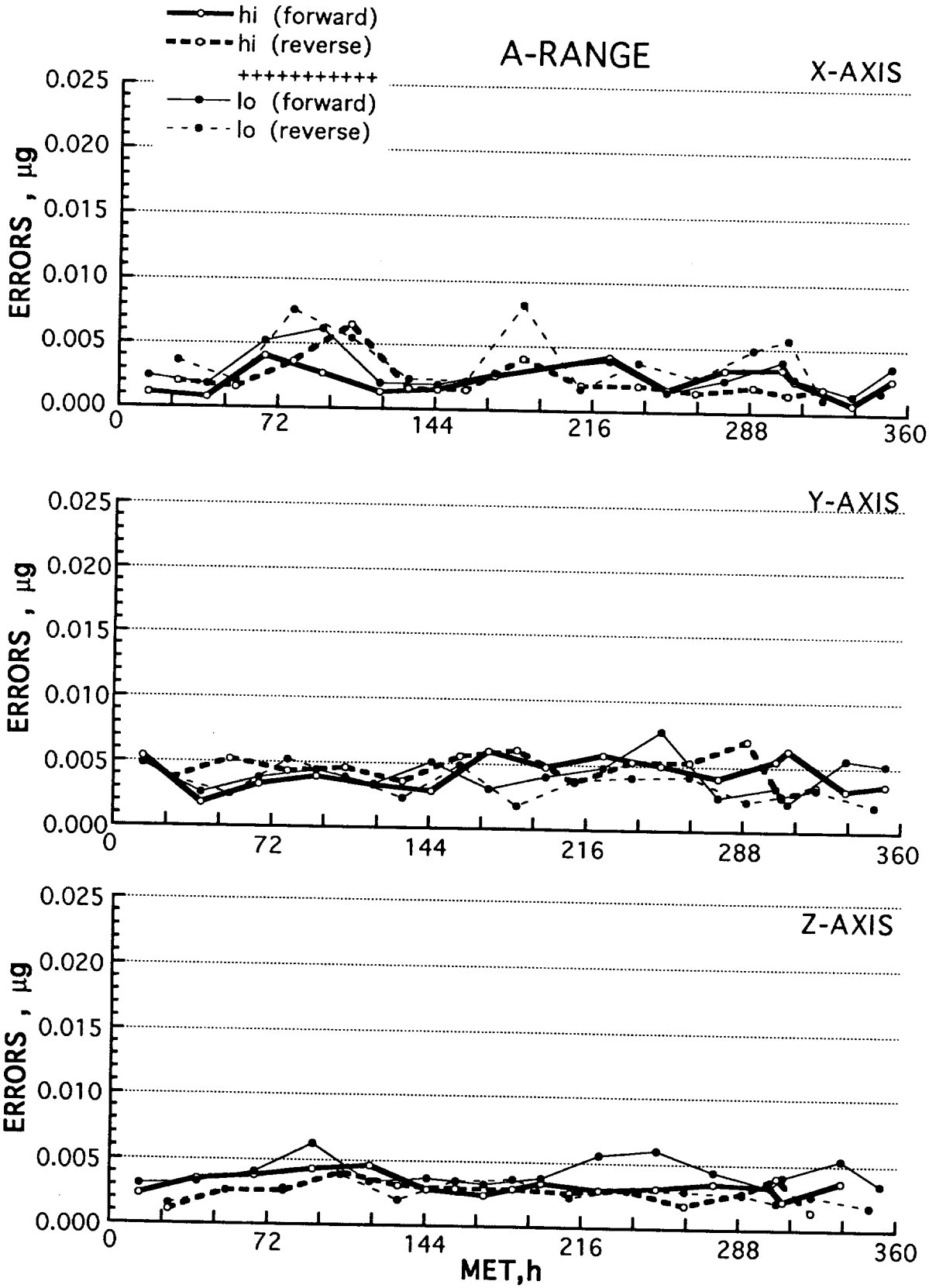

Fig. 34 OARE STS-65 scale factor measurement average errors (A-Range).

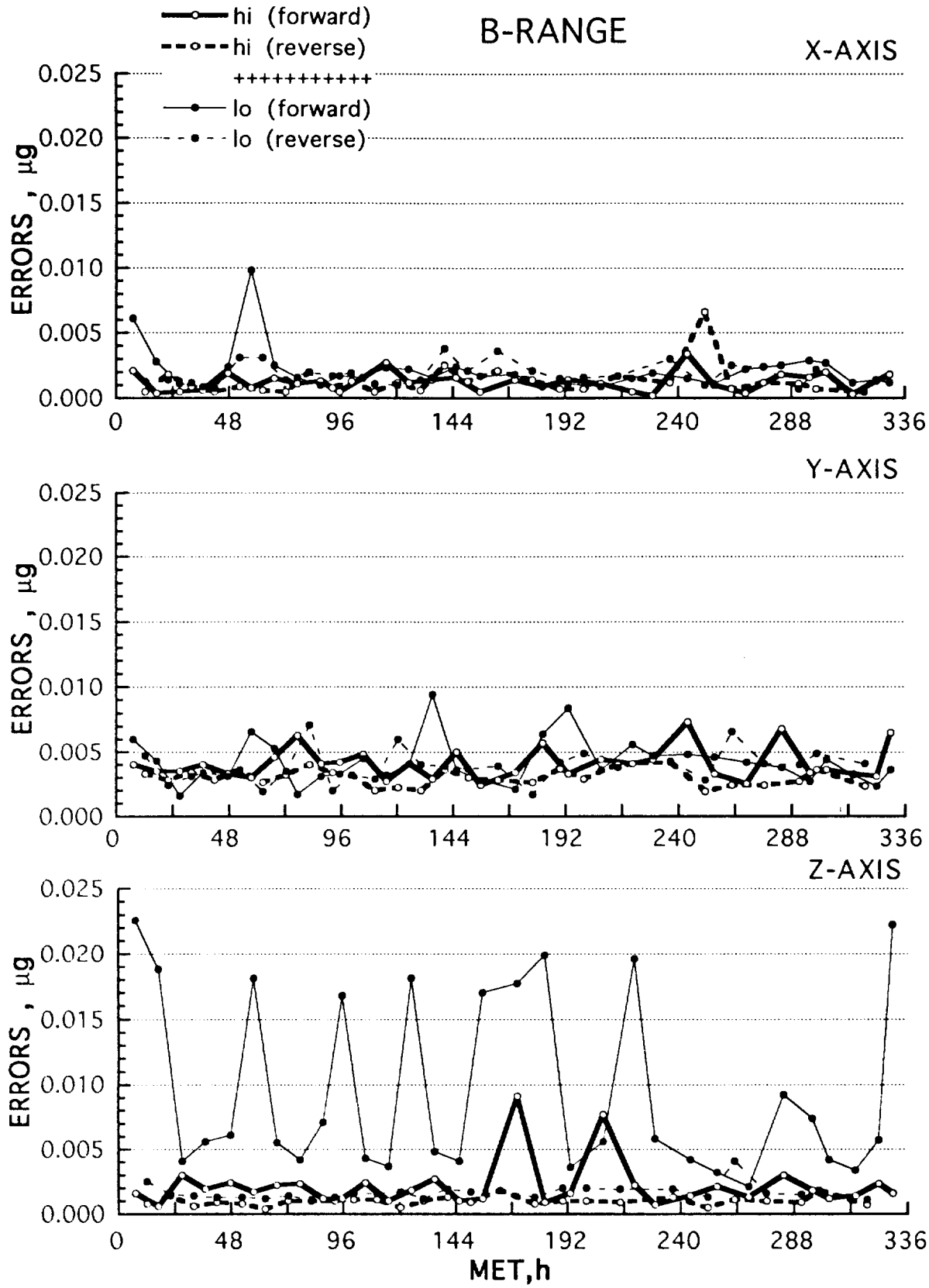

Fig. 35 OARE STS-50 scale factor measurements average errors (B-Range).

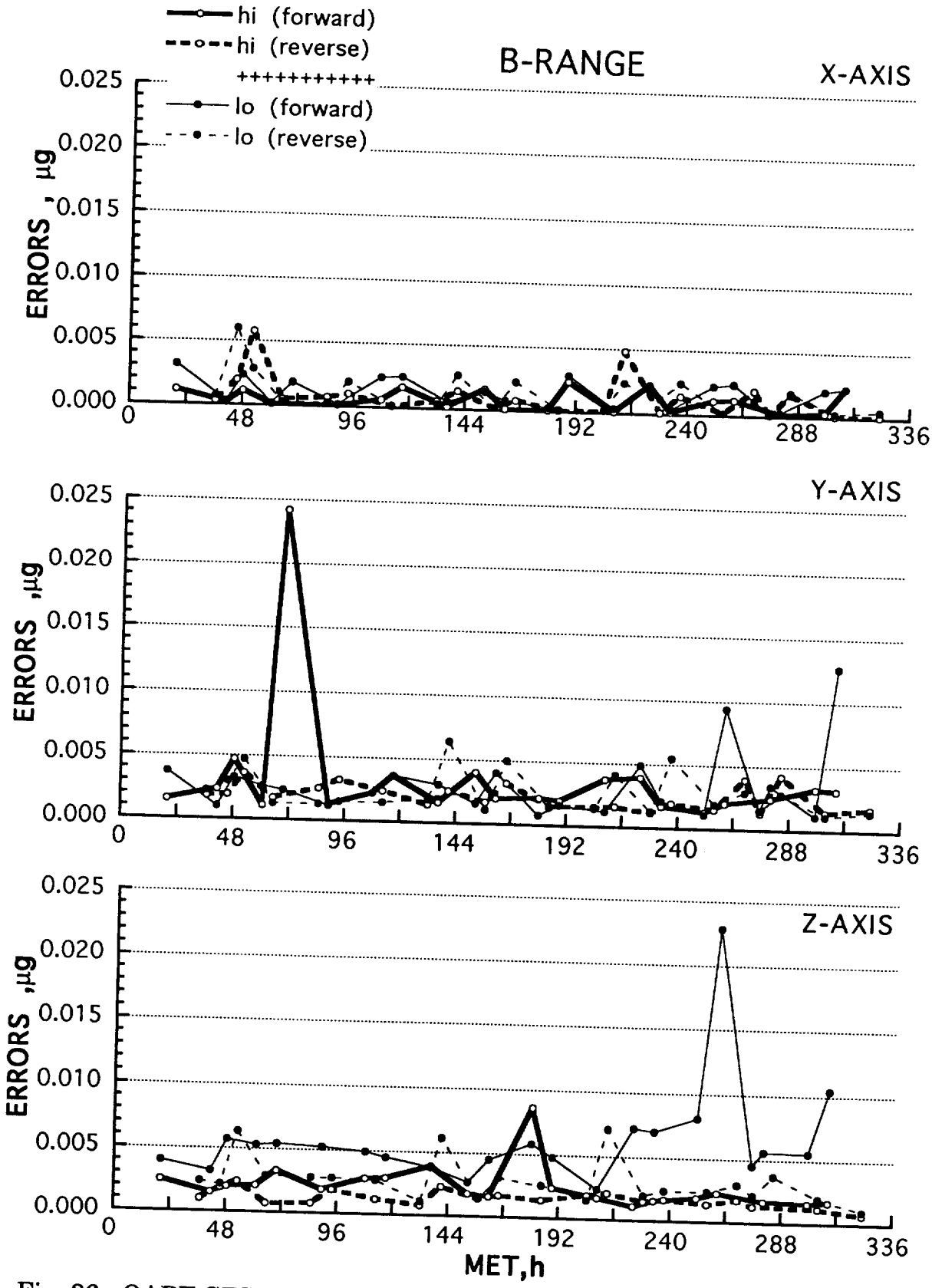

Fig. 36 OARE STS-58 scale factor measurement average errors (B-Range).

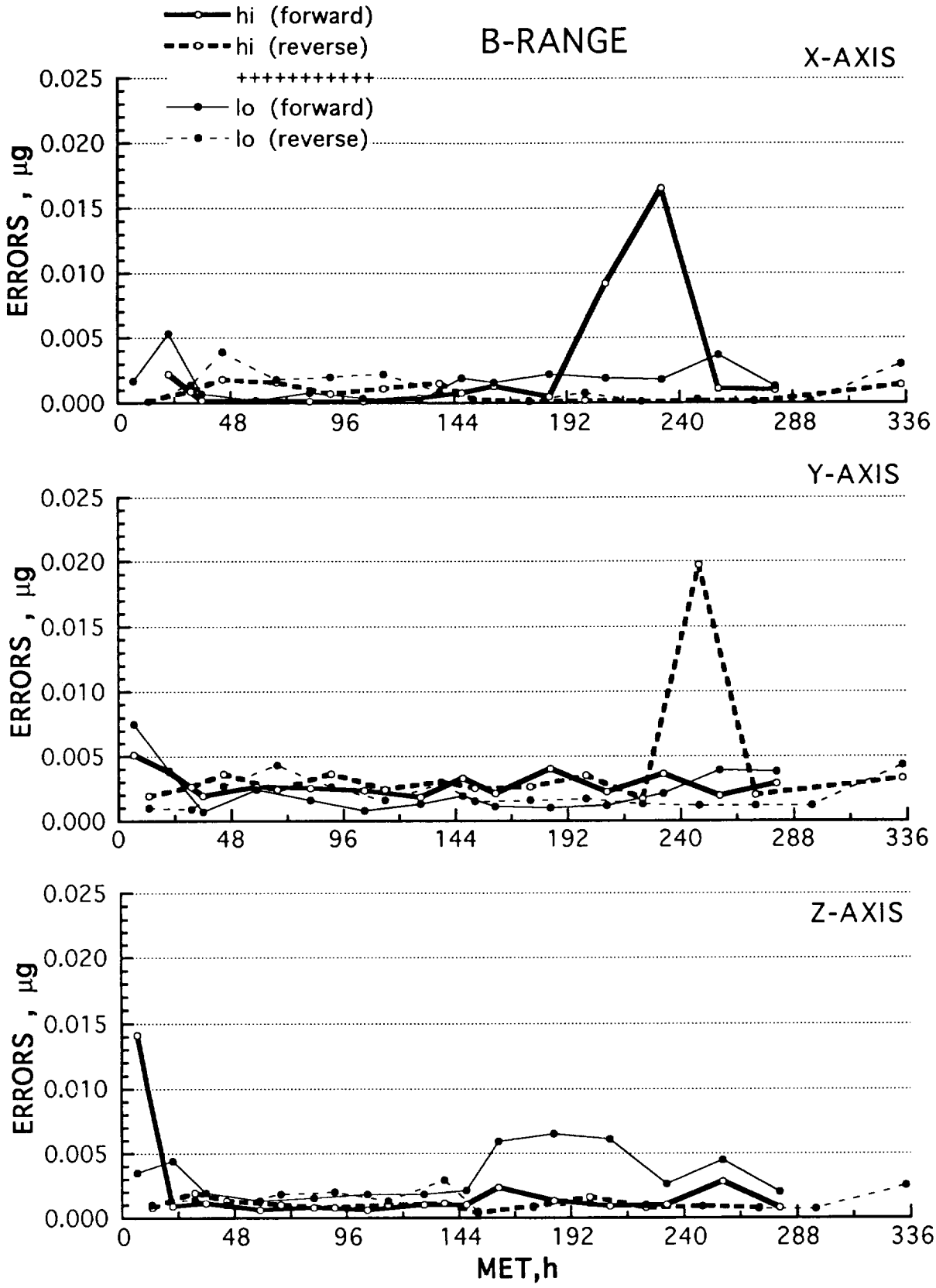

Fig. 37 OARE STS-62 scale factor measurement average errors (B-Range).

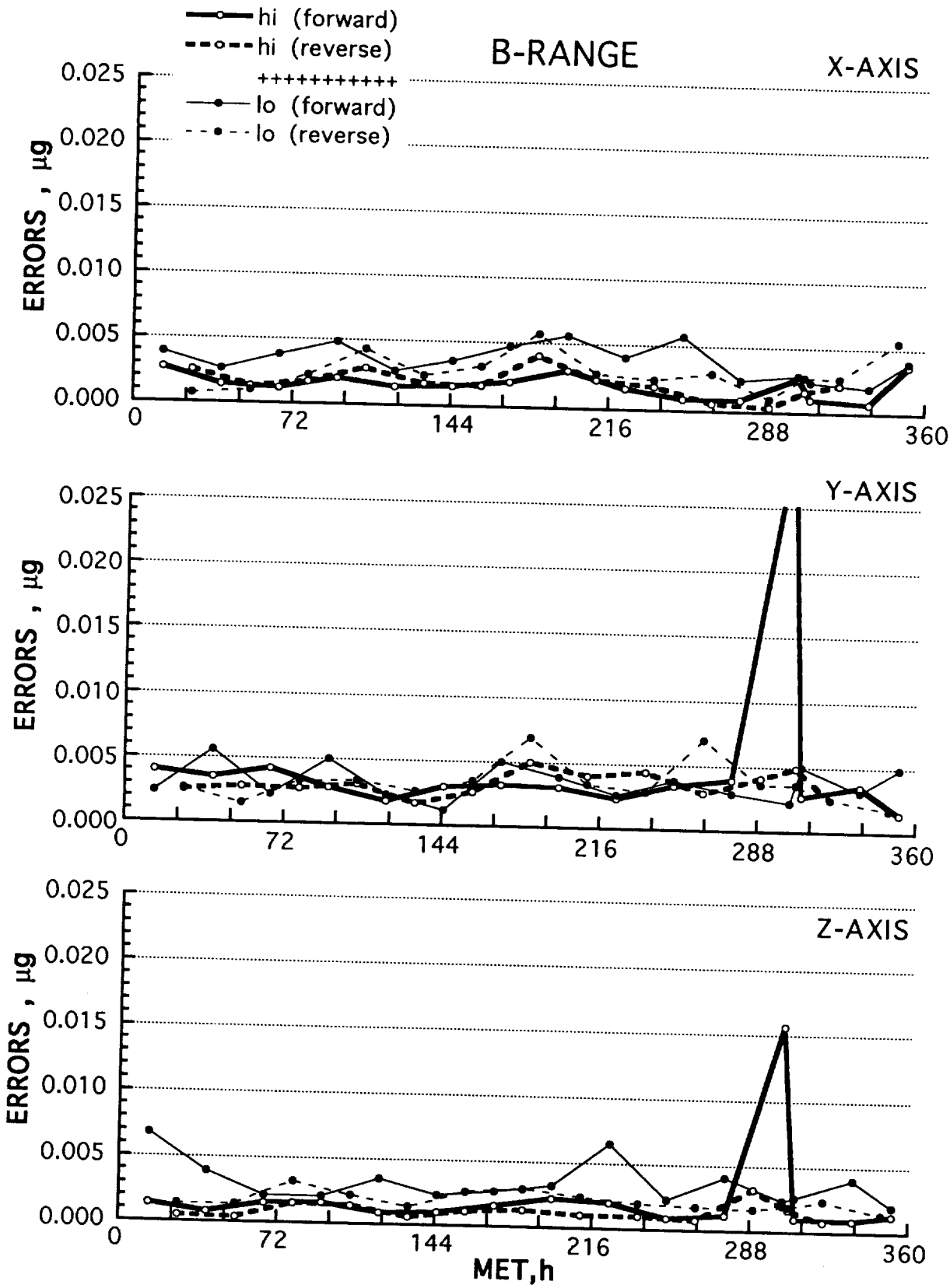

Fig. 38 OARE STS-65 scale factor measurement average errors (B-Range).

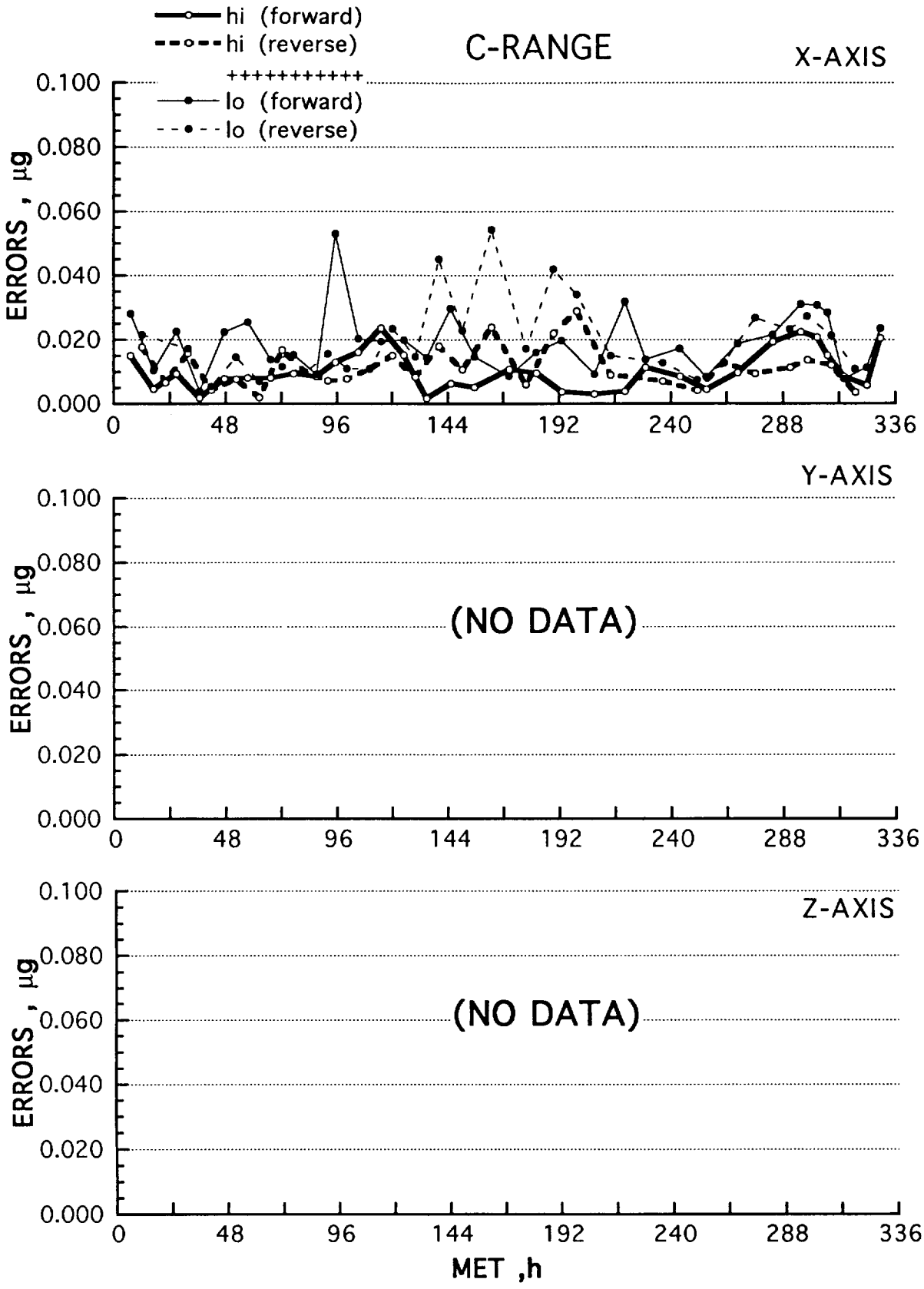

Fig. 39 OARE STS-50 scale factor measurement average errors (C-Range).

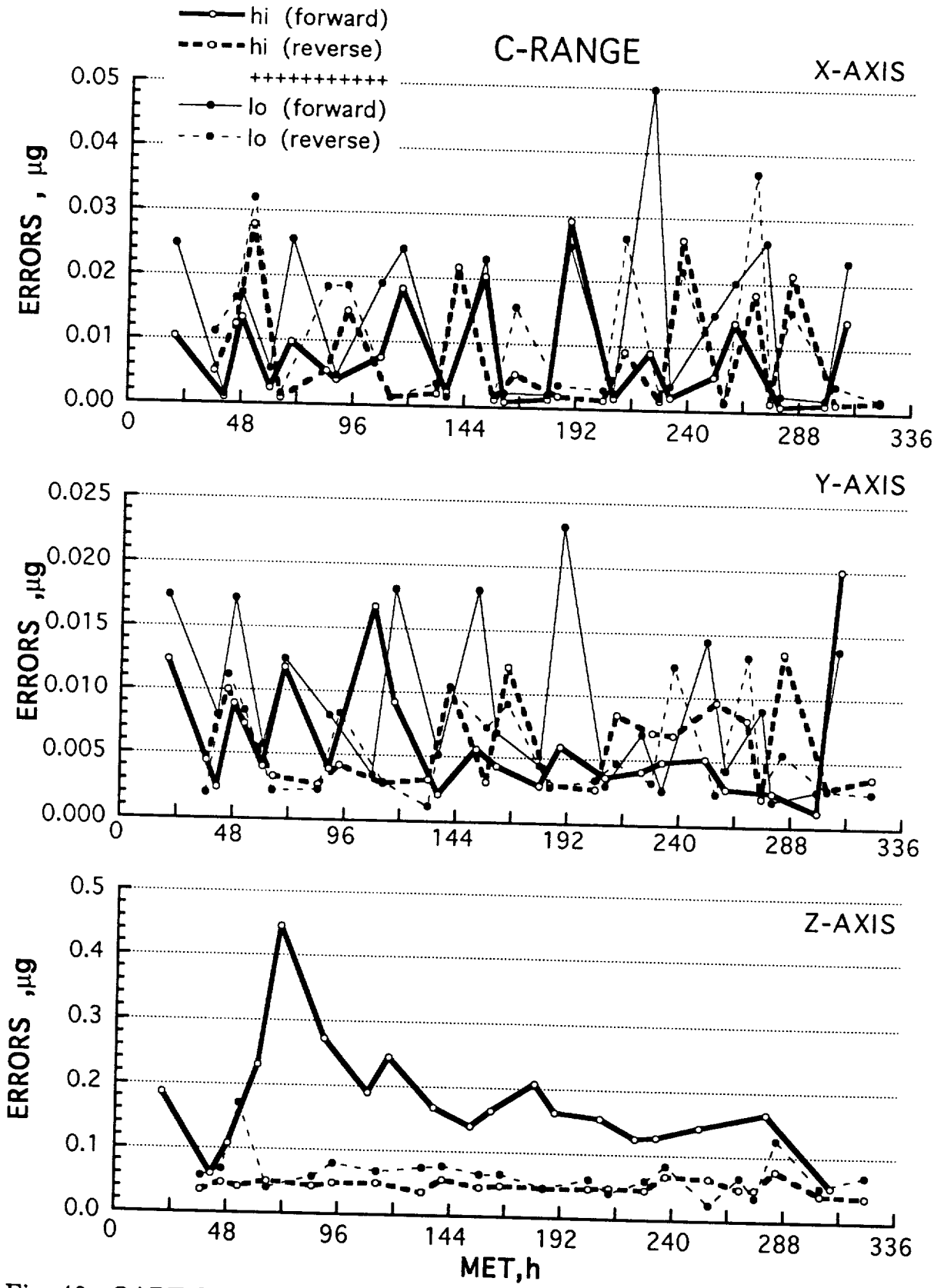

Fig. 40 OARE STS-58 scale factor measurement average errors (C-Range).

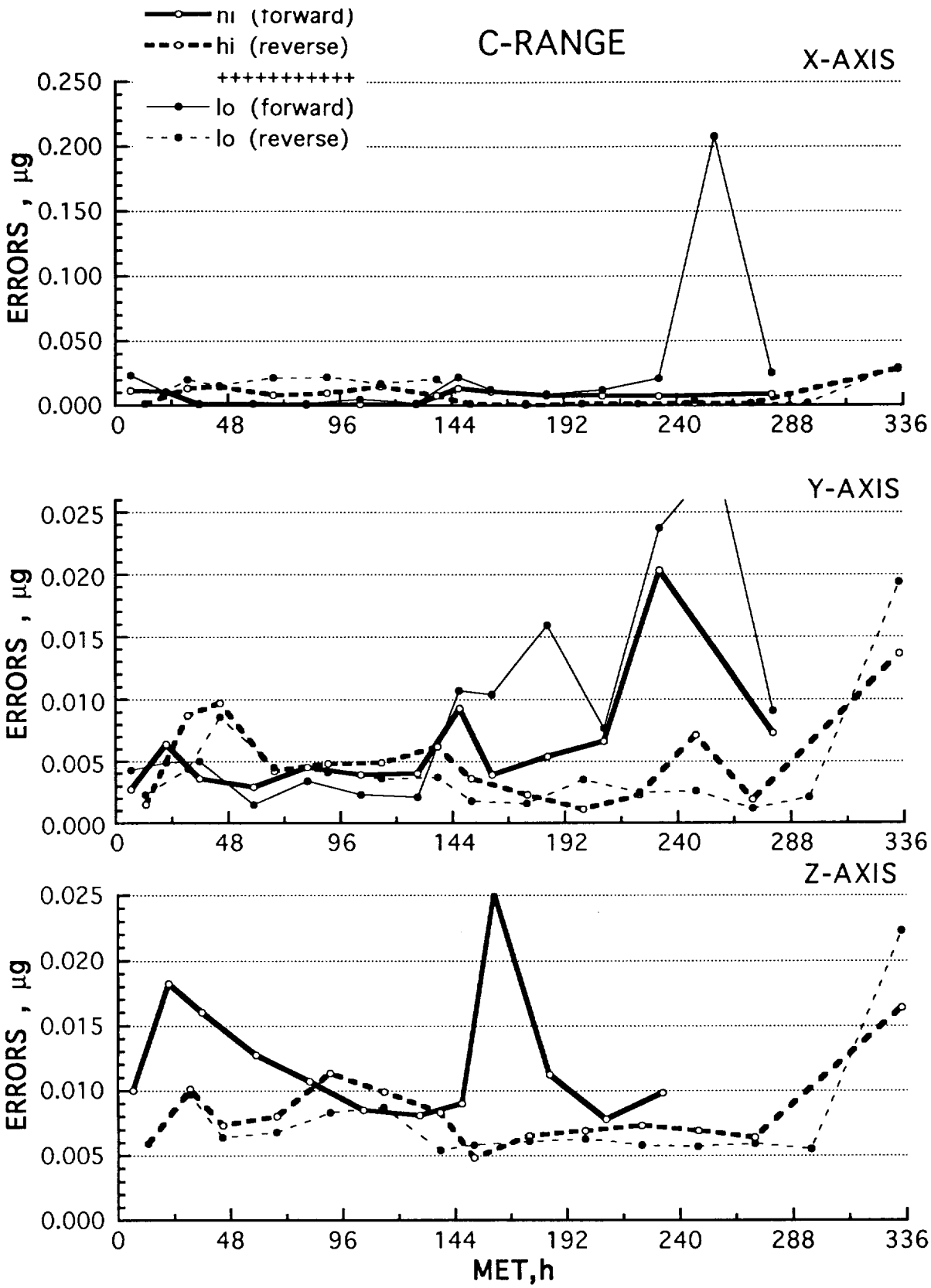

Fig. 41 OARE STS-62 scale factor measurement average errors (C-Range).

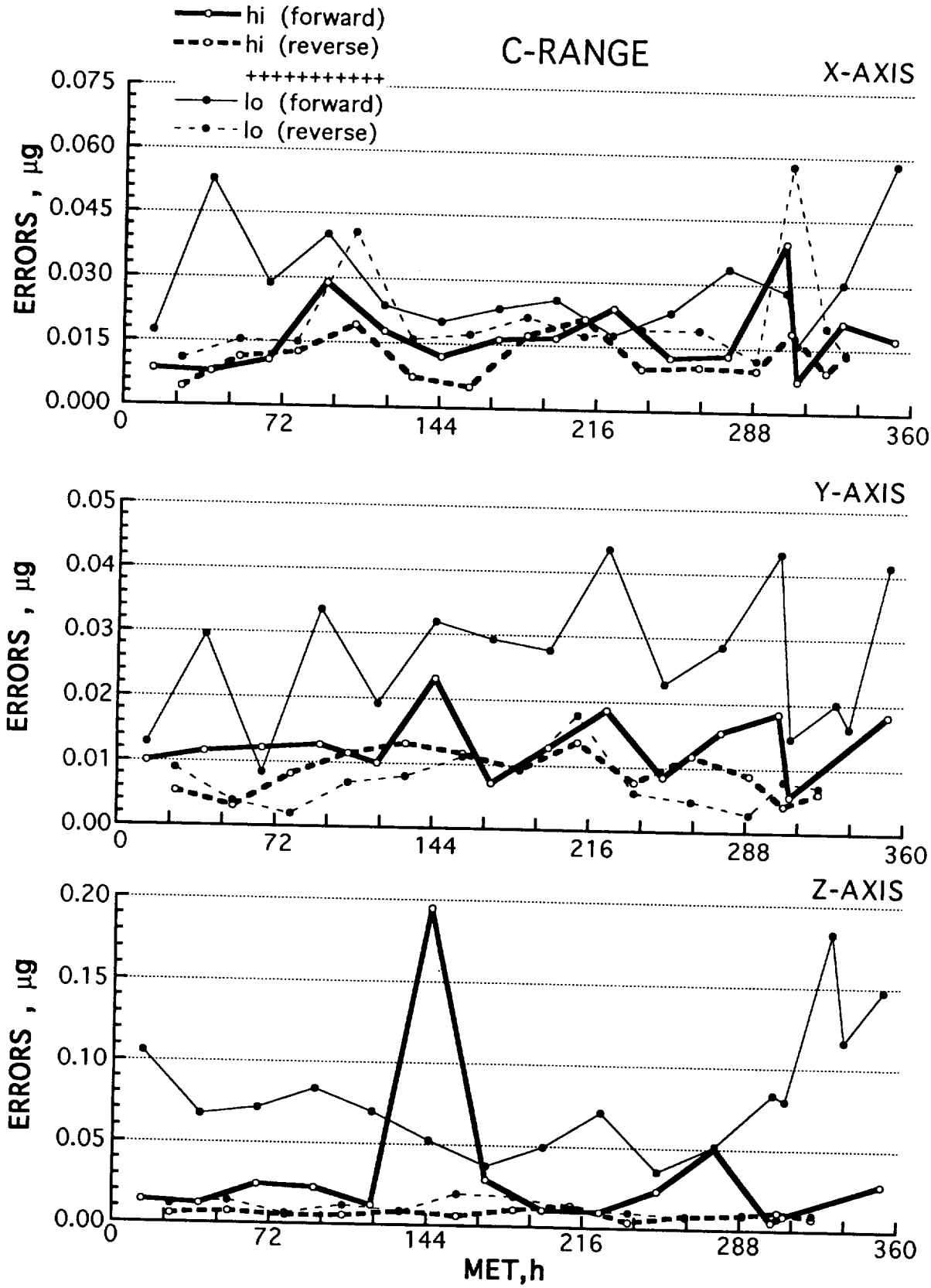

Fig. 42 OARE STS-65 scale factor measurement average errors (C-Range).

REPORT DOCUMENTATION PAGE

Form Approved
OMB No. 0704-0188

1. AGENCY USE ONLY *(Leave blank)*	2. REPORT DATE	3. REPORT TYPE AND DATES COVERED
	January 1995	Technical Memorandum

4. TITLE AND SUBTITLE
Summary of OARE Flight Calibration Measurements

5. FUNDING NUMBERS
242-80-01-01

6. AUTHOR(S)
Robert C. Blanchard and John Y. Nicholson

7. PERFORMING ORGANIZATION NAME(S) AND ADDRESS(ES)
NASA Langley Research Center
Hampton, VA 23681-0001

8. PERFORMING ORGANIZATION REPORT NUMBER

9. SPONSORING / MONITORING AGENCY NAME(S) AND ADDRESS(ES)
National Aeronautics and Space Administration
Washington, DC 20546-0001

10. SPONSORING / MONITORING AGENCY REPORT NUMBER
NASA TM-109159

11. SUPPLEMENTARY NOTES
Blanchard: Langley Research Center, Hampton, VA and Nicholson: ViGYAN, Inc., Hampton, VA

12a. DISTRIBUTION / AVAILABILITY STATEMENT
Unclassified - Unlimited
Subject Category ~~38~~ 34

12b. DISTRIBUTION CODE

13. ABSTRACT ***(Maximum 200 words)***

To date, the Orbital Acceleration Research Experiment (OARE) has flown on the Shuttle Orbiter for five missions; namely, STS-40, STS-50, STS-58, STS-62, and STS-65. The OARE instrument system contains a 3 axis accelerometer which can resolve accelerations to the nano-g (10/-9 g) level and a full calibration station to permit in situ bias and scale factor calibration measurements. This calibration capability eliminates the large uncertainty encountered with accelerometers flown in the past on the Orbiter which use ground-based calibrations to provide absolute acceleration measurements. A detailed flight data report presentation is given for the OARE calibration measurements from all missions, along with an estimate of the calibration errors. The main aim is to collect, process, and present the calibration data in one archival report. These calibration data are the necessary key ingredient to produce the absolute acceleration levels from the OARE acceleration flight data.

14. SUBJECT TERMS
microaccelerometer, flight instrumentation, flight calibration

15. NUMBER OF PAGES
63

16. PRICE CODE
A04

17. SECURITY CLASSIFICATION OF REPORT	18. SECURITY CLASSIFICATION OF THIS PAGE	19. SECURITY CLASSIFICATION OF ABSTRACT	20. LIMITATION OF ABSTRACT
Unclassified	Unclassified		